การเตรียมตัวเร่งปฏิกิริยาโคบอลต์บนเส้นใยซิลิกาโดยอิเล็กโทรสปินนิงสำหรับไฮโดรจิเนชันของ
คาร์บอนมอนอกไซด์

นางสาว สุวดี พรหมดวง

วิทยานิพนธ์นี้เป็นส่วนหนึ่งของการศึกษาตามหลักสูตรปริญญาวิทยาศาสตรมหาบัณฑิต
สาขาวิชาปิโตรเคมีและวิทยาศาสตร์พอลิเมอร์
คณะวิทยาศาตร์ จุฬาลงกรณ์มหาวิทยาลัย
ปีการศึกษา 2553

PREPARATION OF Co/SiO$_2$ FIBER CATALYSTS BY ELECTROSPINNING FOR CO HYDROGENATION

Miss Suwadee Promduang

ศูนย์วิทยทรัพยากร
จุฬาลงกรณ์มหาวิทยาลัย

A Thesis Submitted in Partial Fulfillment of the Requirements

for the Degree of Master of Science Program in Petrochemistry and Polymer Science

Faculty of Science

Chulalongkorn University

Academic year 2010

530607

Thesis Title

PREPARATION OF Co/SiO$_2$ FIBER CATALYSTS BY ELECTROSPINNING FOR CO HYDROGENATION

By

Miss Suwadee Promduang

Field of Study

Petrochemistry and Polymer Science

Thesis Advisor

Assistant Professor Prasert Reubroycharoen.

Accepted by the Faculty of Science, Chulalongkorn University in Partial Fulfillment of the Requirements for the Master's Degree

.... Dean of the Faculty of Science

(Professor Supot Hannongbua, Dr.rer.nat)

THESIS COMMITTEE

.... Chairman

(Professor Pattarapan Prasassarakich, Ph.D.)

.... Thesis Advisor

(Assistant Professor Prasert Reubroycharoen, D.Eng.)

.... Examiner

(Associate Professor Wimonrat Trakarnpruk, Ph.D.)

.... External Examiner

(Assistant Professor Chaiyan Chaiya, Ph.D.)

สุวดี พรหมดวง : การเตรียมตัวเร่งปฏิกิริยาโคบอลต์บนเส้นใยซิลิกาโดยอิเล็ก-โทรสปินนิงสำหรับไฮโดรจิเนชันของคาร์บอนมอนอกไซด์ (PREPARATION OF Co/SiO₂ FIBER CATALYSTS BY ELECTROSPINNING FOR CO HYDROGENATION) อ. ที่ปรึกษาวิทยานิพนธ์หลัก : ผศ.ดร. ประเสริฐ เรียบร้อยเจริญ,87 หน้า.

จุดประสงค์หลักของงานวิจัยนี้คือ การเตรียมตัวเร่งปฏิกิริยาโคบอลต์บนเส้นใยซิลิกา สำหรับไฮโดรจิเนชันของคาร์บอนมอนอกไซด์ ภาวะที่เหมาะสมในการเตรียมเส้นใยซิลิกา คือ ขนาดหัวเข็มเท่ากับ 0.4 มิลลิเมตร, ความเข้มข้นของพอลิเมอร์ที่ใส่ลงไปเท่ากับ ร้อยละ 70 ของ น้ำหนักพอลิเมอร์, ความต่างศักย์ 20 กิโลโวลต์ และ ระยะทางระหว่างปลายเข็มถึงฉากรับ เท่ากับ 15 เซนติเมตร ซึ่งขนาดของเส้นใยที่ได้มีขนาดเส้นผ่านศูนย์กลางเฉลี่ยเท่ากับ 448 นาโน เมตร สามารถวิเคราะห์ด้วยเทคนิค SEM ตัวเร่งปฏิกิริยาโคบอลต์บนเส้นใยซิลิกา สามารถ เตรียมด้วยวิธีการเคลือบสารละลายโคบอลต์แอซีเททที่มีความเข้มข้นของโลหะแตกต่างกัน คือ ร้อยละ 5, 10, 15 และ 20 ของน้ำหนักโลหะแล้วนำไปอบ และเผาที่อุณหภูมิ 600 องศาเซลเซียส เป็นเวลา 2 ชั่วโมง นำตัวเร่งปฏิกิริยาไปพิสูจน์เอกลักษณ์ด้วยเทคนิค SEM, EDS, TEM, XRD and TPR พร้อมทั้งเปรียบเทียบกับตัวเร่งปฏิกิริยาแบบรูพรุน

ตัวเร่งปฏิกิริยานำไปทดสอบการเร่งปฏิกิริยาไฮโดรจิเนชันของคาร์บอนมอนอกไซด์ โดยศึกษาปัจจัยที่มีผลต่อปฏิกิริยา ได้แก่ ตัวรองรับ อุณหภูมิในการเกิดปฏิกิริยา และปริมาณ โลหะโคบอลต์ ผลการทดสอบพบว่า ที่อุณหภูมิในการเกิดปฏิกิริยาที่ 300 องศาเซลเซียส ตัวเร่ง ปฏิกิริยาแบบเส้นใยจะให้ค่าการเปลี่ยนคาร์บอนมอนนอกไซด์เท่ากับร้อยละ 19.75 ตัวเร่ง และ ค่าการเลือกเกิดมีเทนเท่ากับร้อยละ 88.39 ซึ่งสูงกว่าตัวเร่งปฏิกิริยาแบบรูพรุน แต่ค่าการเลือก เกิดคาร์บอนไดออกไซด์จะต่ำกว่า เนื่องจากตัวเร่งปฏิกิริยาแบบเส้นใยดูดซับน้ำบนพื้นผิวได้ น้อย ทำให้ตัวเร่งปฏิกิริยาแบบเส้นใยเกิดปฏิกิริยาวอร์เตอร์ก๊าซชิฟลดลง ผลของปริมาณ โคบอลต์ที่เคลือบลงบนเส้นใยซิลิกา พบว่าตัวเร่าปฏิกิริยาที่มีปริมาณโคบอลต์ร้อยละ 10 เป็น ตัวเร่งปฏิกิริยาที่ดีที่สุดสำหรับปฏิกิริยาไฮโดรจิเนชันของคาร์บอนมอนอกไซด์

สาขาวิชา.ปิโตรเคมีและวิทยาศาสตร์พอลิเมอร์ ลายมือชื่อนิสิต...สุวดี พรหมดวง...............

ปีการศึกษา 2553   ลายมือชื่อ อ.ที่ปรึกษาวิทยานิพนธ์หลัก.........

5072536323 : MAJOR   PETROCHEMISTRY AND POLYMER SCIENCE
KEYWORDS :   ELECTROSPINNING / SOL-GEL / FIBER CATALYST / FISCHER-TROPSCH

SUWADEE PROMDUANG: PREPARATION OF Co/SiO$_2$ FIBER CATALYSTS BY ELECTROSPINNING FOR CO HYDROGENATION. THESIS ADVISOR: ASST. PROF. PRASERT REUBROYCHAREON,Ph.D., 87 pp.

The aim of this work is to prepare cobalt/silica fiber catalysts via electrospinning technique for CO hydrogenation. The optimum condition for fiber electrospinning was needle size of 0.4 mm, PVP content of 70wt%, voltage of 20 kV and the tip to collector distance of 15 cm. At the optimum condition, the diameter of the fiber was smallest at diameter of 448 nm, analyzed by SEM technique. The cobalt/silica fiber catalyst was prepared by impregnation method using cobalt acetate as a source of cobalt at various loading percentages (5, 10, 15 and 20wt% of metal loading). The cobalt/silica fiber catalysts were characterized by SEM/EDS, BET, TEM, XRD, TPR, and activity test for comparing to the conventional porous catalyst, cobalt/silica porous catalyst.

The catalyst activity tests on CO hydrogenation over the fiber and porous catalysts were studied by following effects, support, reaction temperature, and cobalt contents. The operated temperature in CO hydrogenation was at 300°C, with %CO conversion of 19.75 and % methane selectivity of 88.35, higher than that of porous catalyst. And, the selectivity of carbon dioxide was lower than the porous catalyst, indicated the fiber catalysts was demoted the water gas shift reaction by decreasing the water absorbed on the fiber catalyst surface. The results on the effect of cobalt loading showed that 10%Co/SiO$_2$ fiber catalyst was the best catalyst for CO hydrogenation in this study.

Field of Study : Petrochemistry and Polymer Science   Student's Signature ....

Academic Year : 2010   Advisor's Signature ....

ACKNOWLEDGEMENTS

ศูนย์วิทยทรัพยากร
จุฬาลงกรณ์มหาวิทยาลัย

CONTENTS

ศูนย์วิทยทรัพยากร
จุฬาลงกรณ์มหาวิทยาลัย

LIST OF TABLES

LIST OF FIGURES

LIST OF ABBREVIATION

Co	cobalt
SiO_2	silicon dioxide
CO	carbon monoxide
mm	millimeter (s)
wt%	weight percent
kV	kilovoltage (s)
cm	centimeter (s)
^oC	degree Celsius
nm	nanometer
SEM	Scanning electron microscope
EDS	Energy dispersive spectroscopy
TEM	Transmission electron microscopy
XRD	X-ray Diffraction
TPR	Temperature-programmed reduction
FTS	Fischer-Tropsch synthesis
atm	atmosphere
mL	milliliter
min	minute (s)
g	gram (s)
i.e	that is
Eq.	equation
et. al	and others
DC	direct current
$ohm^{-1}W^{-1}$	ratio of electric conductivity per ohm and watt
h	hour (s)
FESEM	Field Emission Scanning Electron Microscopy
^oF	degree Fahrenheit
PVA	poly(vinyl alcohol)
mol	mole
TEOS	tetraethyl orthosilicate

IR	infrared spectroscopy
DSC	differential scanning calorimetry
TGA	thermogravimetric Analysis
FT-IR	fourier transform infrared spectroscopy
WAXD	wide angle X-ray scattering
TG- DTA	thermogravimetry-differential thermalgravimetric analysis
P	pressure
MPa	megapascal
T	temperature
V	volume
DRIFT	diffuse reflectance infrared Fourier transform spectroscopy
cat	catalyst
GC	Gas Chromatograph
HCl	hydrochloric acid
TCD	tip to collector distance
He	helium
TCD	thermal conduct detector
PVP	polyvinylpyrrolidone
μm	micron
MW	molecular weight
EtOH	ethanol
No.	number
cm^3	cubic centimeter

CHAPTER I

INTRODUCTION

1.1 Statement of problem

       Nowsday, the unstable of gasoline price in the world market directly affects to our country. Because most of energy in Thailand are importing from abroad. Now so many Thai researchers are trying to study about the alternative energy which can be produce in our country for decreasing the importing. Synthetic fuel derived from Fischer-Tropsch synthesis (FTS) which is clean energy is very interesting. FTS was directly converted coal gasifier gas or natural gas into higher hydrocarbons [1]. The cobalt-based catalysts which are the commercial catalysts are very important and very good for the attracted most of the current attention for the directed conversion of syngas in FTS. This may caused of their high activity, high selectivity for long chain paraffins, and low activity in water gas shift reaction. Beside cobalt, some supports such as SiO_2 were indispensable. The chemical and textural properties of the cobalt catalyst support effected to the catalytic activity and product selectivity. High reducibility, high dispersion well-fined phase of cobalt was required [2]. Most of available catalyst always are porous catalyst but they have some disadvantages. The condensation of products may block catalyst pores bring to the deactivated and the pressure drop in catalyst. So to solve this problem using of electrospinning techniques with sol-gel to prepare fiber catalysts are now focusing on [3].

       This research can be divided into two main experimental parts. The first part, we have studied the effect of many factors such as polymer content, needle size, the tip to collector distance, voltage value and cobalt content in preparation of Co/SiO_2 fiber catalysts by electrospinning technique and impregnation. The second part, we have studied the performance of fibers catalyst impregnated with cobalt acetate for Fischer-Tropsch synthesis.

1.2 Objective

1. To prepare Co/SiO_2 fiber catalyst by electrospinning technique.
2. To find optimum condition for electrospinning technique.
3. To study the performance of fiber catalyst impregnated with cobalt acetate for Fischer-Tropsch synthesis.

1.3 Scope of the research

The research procedures were carried out as follows:

1. Literature review.
2. Study of Fischer-Tropsch synthesis apparatus in laboratory scale, and preparation of the chemicals and raw materils for the experiment.
3. Study of the preparation conditions of silica fiber by electrospinning technique and characterization.
4. Study of influence of cobalt/silica fiber catalyst and operating parameter on the performance in the Fischer-Tropsch synthesis.

CHAPTER II

THEORY AND LITERATURE REVIEWS

2.1 Sol-gel process

Sol- gel process [4] that has, in the past years, gained much notoriety in the glass and ceramic fields is the sol-gel reaction. This chemistry produces a variety of inorganic networks from silicon or metal alkoxide monomer precursors. Although first discovered in the late 1800s and extensively studied since the early 1930s, a renewed interest surfaced in the early 1970s when monolithic inorganic gels were formed at low temperatures and converted to glasses without a high temperature melting process. Through this process, homogeneous inorganic oxide materials with desirable properties of hardness, optical transparency, chemical durability, tailored porosity, and thermal resistance, can be produced at room temperatures, as opposed to the much higher melting temperatures required in the production of conventional inorganic glasses. The specific uses of these sol-gel produced glasses and ceramics are derived from the various material shapes generated in the gel state, i.e., monoliths, films, fibers, and monosized powders. Many specific applications include optics, protective and porous films, optical coatings, window insulators, dielectric and electronic coatings, high temperature superconductors, reinforcement fibers, fillers, and catalysts.
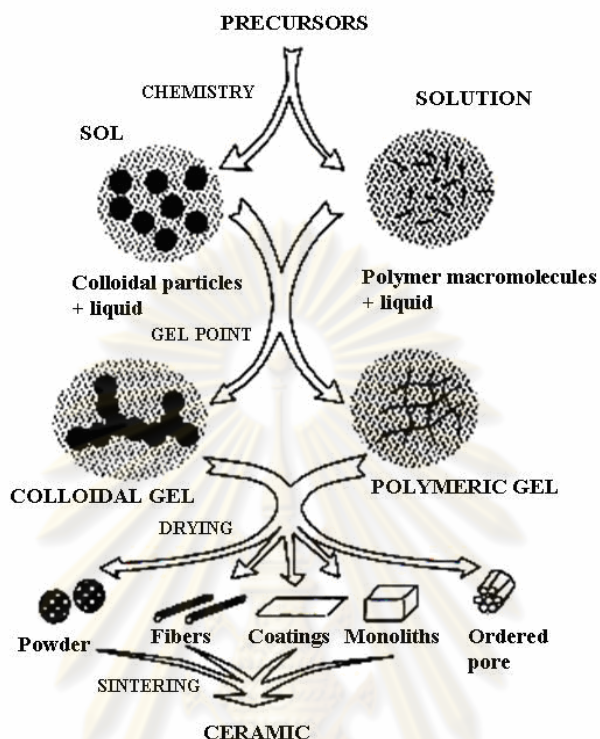
Figure 2.1 Simplified chart of sol-gel processes [5].

2.1.1 Sol-gel chemistry of metal alkoxide

Metal alkoxides are popular precursors because they react readily with water. The reaction is called hydrolysis, because a hydroxyl ion becomes attached to the metal atom, as in the following reaction (Eq. 2.1) [6, 7].

$$Si(OR)_4 + 4H_2O \quad \text{----------}> \quad Si(OH)_4 + 4R\text{-}OH \qquad (2.1)$$

Two partially hydrolyzed molecules can link together in a condensation reaction (Eq. 2.2, 2.3).

$$(OR)_3Si\text{-}OH + HO\text{-}Si(OR)_3 \text{----------}> (OR)_3Si\text{-}O\text{-}Si(OR)_3 + H_2O \quad (2.2)$$

$$(OR)_3Si\text{-}OR + HO\text{-}Si(OR)_3 \text{----------}> (OR)_3Si\text{-}O\text{-}Si(OR)_3 + ROH \quad (2.3)$$
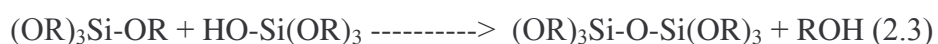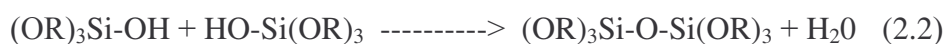
The products can contain one or more metal atoms in the same molecule depending on the relative hydrolysis and condensation reaction rates of the component metal alkoxides. The more alkoxides present in the original mixture the more complex can the polymerization become. Ultimately, the polymeric products become insoluble due to cross-linking and gellation or precipitation results. The complexity of a multicomponent system makes investigation of the reaction mechanisms extremely difficult. Brinker and Scherer give an excellent summary of research in this field and describe their own extensive investigations on polymer growth and gel formation.

2.2 Electrospinning

Electrospinning process [8] was patented, wherein an experimental setup was outlined for the production of polymer filaments using electrostatic force. When used to spin fibers this way, the process is termed as electrospinning. In other words, electrospinning is a process that creates nanofibers through an electrically charged jet of polymer solution or polymer melt. Following this, investigations of the process have been carried out by a number of researchers. The electrospinning process, in its simplest form consisted of a pipette to hold the polymer solution, two electrodes and a DC voltage supply in the kV range, Figure. 2.2. The polymer drop from the tip of the pipette was drawn into a fiber due to the high voltage. The jet was electrically charged and the charge caused the fibers to bend in such a way that every time the polymer fiber looped, its diameter was reduced. The fiber was collected as a web of fibers on the surface of a grounded target as shown in Figure. 2.2.
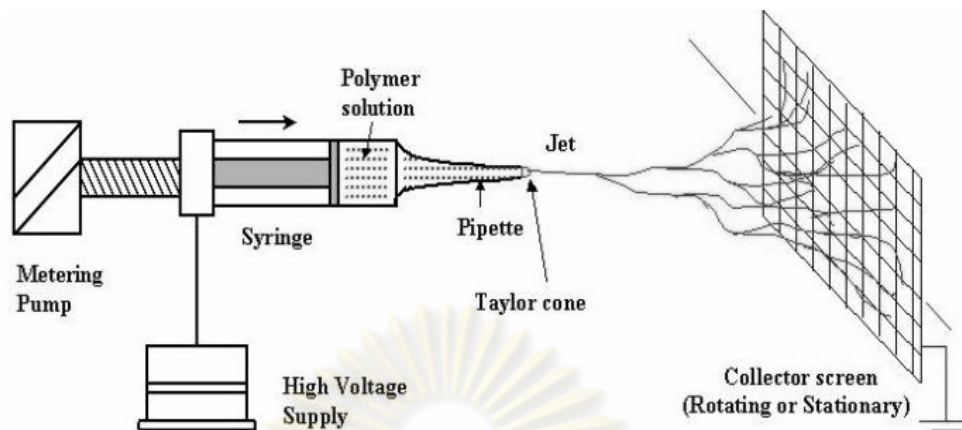
Figure 2.2 Diagram of electrospinning process [9].

Important features of electrospinning are:

a. Suitable solvent should be available for dissolving the polymer.

b. The vapor pressure of the solvent should be suitable so that it evaporates quickly enough for the fiber to maintain its integrity when it reaches the target but not too quickly to allow the fiber to harden before it reaches the nanometer range.

c. The viscosity and surface tension of the solvent must neither be too large to prevent the jet from forming nor be too small to allow the polymer solution to drain freely from the pipette.

d. The power supply should be adequate to overcome the viscosity and surface tension of the polymer solution to form and sustain the jet from the pipette.

e. The gap between the pipette and grounded surface should not be too small to create sparks between the electrodes but should be large enough for the solvent to evaporate in time for the fibers to form.

2.2.1 The electrospinning process parameters

2.2.1.1 Solution property

In order to carry out electrospinning, the polymer must first be in a liquid form, either as molten polymer or as polymer solution. The property of the solution

plays a significant part in the electrospinning process and the resultant fiber morphology. During the electrospinning process, the polymer solution will be drawn from the tip of the needle. The electrical property of the solution, surface tension and viscosity will determine the amount of stretching of the solution. The rate of evaporation will also have an influence on the viscosity of the solution as it is being stretched. The solubility of the polymer in the solvent not only determines the viscosity of the solution but also the types of polymer that can be mixed together.

2.2.1.2 Surface tension

In electrospinning, the charges on the polymer solution must be high enough to overcome the surface tension of the solution. As the solution jet accelerates from the tip of the source to the collector, the solution is stretched while surface tension of the solution may cause the solution to breakup into droplets. When droplets are collected, a different process called electrospraying is taking place rather than electrospinning, where fibers are collected instead. Surface tension has also been attributed to the formation of beads on the electrospun fibers. Thus it is important to understand the role of surface tension in a fluid. When a very small drop of water falls through the air, the droplet generally takes up a spherical shape. The liquid surface property that causes this phenomenon is known as surface tension. For a liquid molecule submerged within the solution, there is uniform attractive forces exerted on it be other liquid molecules surrounding it. However, for a liquid molecule at the surface of the solution, there is a net downward force as the liquid molecules below exert a greater attractive force than the gas molecules above. Thus the surface is in tension and this causes a contraction at the surface of the solution, which is balanced by repulsive forces that arise from the collisions of molecules from the interior of the solution. The net effect of the pulling of all the surface liquid molecules causes the liquid surface to contract thereby reducing the surface area. Therefore, for a droplet of water, a spherical shape is the lowest surface area to volume ratio.

2.2.1.3 Viscosity

The viscosity of the solution has a profound effect on electrospinning and the resultant fiber morphology. Generally, the viscosity of the solution is related to the

extent of polymer molecule chains entanglement within the solution. When the viscosity of the solution is too low, electrospraying may occur and polymer particles are formed instead of fibers. At lower viscosity where generally the polymer chain entanglements are lower, there is a higher likelihood that beaded fibers are obtained instead of smooth fibers. Therefore, factors that affect the viscosity of the solution will also affect the electrospinning process and the resultant fibers.

2.2.1.4 Volatility (evaporation)

During the electrospinning process, the solvent will evaporate as the electrospinning jet accelerates towards the collector. When most of the solvents have evaporated when the jet reaches the collector, individual fibers are formed. However, if the rate of evaporation of the solvent is too low such that the solution has not evaporated sufficiently when the electrospinning jet reaches the collector, fibers may not be formed at all and a thin film of polymer solution are deposited on the collector.

The evaporation rate of a solvent is dependent on many factors:

- Vapor pressure
- Boiling point
- Specific heat
- Enthalpy and heat of vaporization of the solvent
- Rate of heat supply
- Interaction between solvent molecules and between solvent and solute molecules
- Surface tension of liquid
- Air movement above the liquid surface

2.2.1.1.4 Conductivity

For electrospinning process to be initiated, the solution must gain sufficient charges such that the repulsive forces within the solution are able to overcome the surface tension of the solution. Subsequent stretching or drawing of the electrospinning jet is also dependent on the ability of the solution to carry charges. Generally, the electric conductivity of solvents is very low (typically between 10^{-3} to

10^{-9} ohm^{-1}W^{-1}) as they contain very few free ions, if any, which are responsible for the electric conductivity of solution. The presence of acids, bases, salts and dissolved carbon dioxide may increase the conductivity of the solvent. The electrical conductivity of the solvent can be increased significantly through mixing chemically non-interacting components. Substances that can be added to the solvent to increase its conductivity includes mineral salts, mineral acids, carboxylic acids, some complexes of acids with amines, stannous chloride and some tetraalkylammonium salts. For organic acid solvents, the addition of a small amount of water will also greatly increase its conductivity due to ionization of the solvent molecules.

2.2.2 Process conditions

Another important parameter that affects the electrospinning process is the various external factors exerting on the electrospinning jet. This includes the voltage supplied, the feedrate, temperature of the solution, type of collector, diameter of needle and distance between the needle tip and collector. These parameters have a certain influence in the fiber morphology although they are less significant than the solution parameters.

2.2.2.1 Voltage

The high voltage will induce the necessary charges on the solution and together with the external electric field, will initiate the electrospinning process when the electrostatic force in the solution overcomes the surface tension of the solution. Generally, both high negative or positive voltage of more than 6kV is able to cause the solution drop at the tip of the needle to distort into the shape of a Taylor Cone during jet initiation. Depending on the feedrate of the solution, a higher voltage may be required so that the Taylor Cone is stable. The columbic repulsive force in the jet will then stretch the viscoelastic solution. If the applied voltage is higher, the greater amount of charges will cause the jet to accelerate faster and more volume of solution will be drawn from the tip of the needle. This may result in a smaller and less stable Taylor Cone. When the drawing of the solution to the collection plate is faster than the supply from the source, the Taylor Cone may recede into the needle. As both the voltage supplied and the resultant electric field have an influence in the stretching and

the acceleration of the jet, they will have an influence on the morphology of the fibers obtained. In most cases, a higher voltage will lead to greater stretching of the solution due to the greater columbic forces in the jet as well as the stronger electric field. These have the effect of reducing the diameter of the fibers and also encourage faster solvent evaporation to yield drier. When a solution of lower viscosity is used, a higher voltage may favor the formation of secondary jets during electrospinning. This has the effect of reducing the fiber diameter. At a lower voltage, the reduced acceleration of the jet and the weaker electric field may increase the flight time of the electrospinning jet which may favor the formation of finer fibers. In this case, a voltage close to the critical voltage for electrospinning may be favorable to obtain finer fibers. At a higher voltage, it was found that there is a greater tendency for beads formation. It was also reported that the shape of the beads changes from spindle-like to spherical-like with increasing voltage. Given the increased stretching of the jet due to higher voltage, there should be less beads formation as reported in some cases as shown in Figure 2.3. The increased in beads density due to increased voltage may be the result of increased instability of the jet as the Taylor Cone recedes into the syringe needle. In an interesting observation, reported that increasing voltage will increased the beads density, which at an even higher voltage, the beads will join to form a thicker diameter fiber.
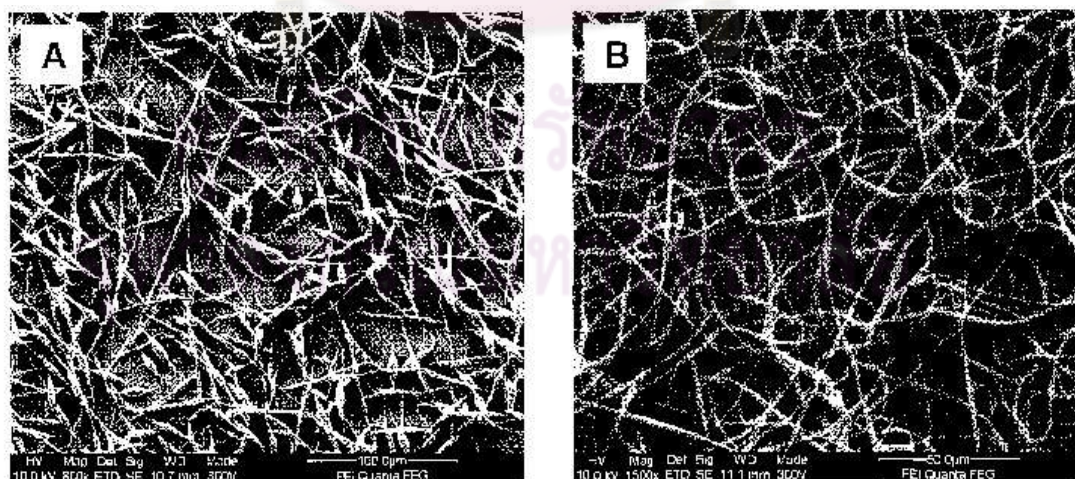
Figure 2.3 Polycaprolactone fibers with [A] beads for electrospinning at a voltage of 6kV and [B] beadless fibers at 22kV [8].

2.2.2.2 Feed rate

The feed rate will determine the amount of solution available for electrospinning. For a given voltage, there is a corresponding feed rate if a stable Taylor cone is to be maintained. When the feed rate is increased, there is a corresponding increase in the fiber diameter or beads size as shown in Figure. 2.4 This is apparent as there is a greater volume of solution that is drawn away from the needle tip However, there is a limit to the increase in the diameter of the fiber due tohigher federate. If the feed rate is at the same rate which the solution is carried away by the electrospinning jet, there must be a corresponding increased in charges when the feed rate is increased. Thus there is a corresponding increased in the stretching of the solution which counters the increased diameter due to increased volume.
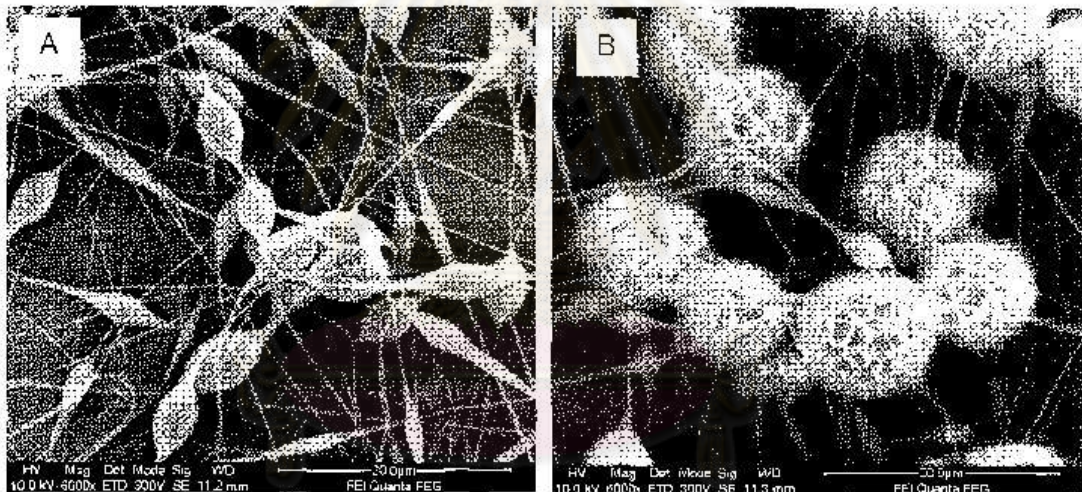
Figure 2.4 Polycaprolactone fibers with increasing beads size with increasing feedrate at [A] 0.5ml/hr and [B] 2ml/hr [8].

Due to the greater volume of solution drawn from the needle tip, the jet will takes a longer time to dry. As a result, the solvents in the deposited fibers may not have enough time to evaporate given the same flight time. The residual solvents may cause the fibers to fuse together where they make contact forming webs. A lower feedrate is more desirable as the solvent will have more time for evaporation.

2.2.2.3 Temperature

The temperature of the solution has both the effect of increasing its evaporation rate and reducing the viscosity of the polymer solution. When polyurethane is electrospun at a higher temperature, the fibers produced have a more uniform diameter. This may be due to the lower viscosity of the solution and greater solubility of the polymer in the solvent which allows more even stretching of the solution. With a lower viscosity, the Columbic forces are able to exert a greater stretching force on the solution thus resulting in fibers of smaller diameter. Increased polymer molecules mobility due to increased temperature also allows the Columbic force to stretch the solution further. However, in cases where biological substances such as enzymes and proteins are added to the solution for electrospinning, the use of high temperature may cause the substance to lose its functionality.

2.2.2.4 Diameter of needle

The internal diameter of the needle has a certain effect on the electrospinning process. A smaller internal diameter was found to reduce the clogging as well as the amount of beads on the electrospun fibers. The reduction in the clogging could be due to less exposure of the solution to the atmosphere during electrospinning. Decrease in the internal diameter of the orifice was also found to cause a reduction in the diameter of the electrospun fibers. When the size of the droplet at the tip of the orifice is decreased, such as in the case of a smaller internal diameter of the orifice, the surface tension of the droplet increases. For the same voltage supplied, a greater columbic force is required to cause jet initiation. As a result, the acceleration of the jet decreases and this allows more time for the solution to be stretched and elongated before it is collected. However, if the diameter of the orifice is too small, it may not be possible to extrude a droplet of solution at the tip of the orifice.

2.2.2.5 Distance between tip and collector

In several cases, the flight time as well as the electric field strength will affect the electrospinning process and the resultant fibers. Varying the distance between the tip and the collector will have a direct influence in both the flight time and the electric field strength. For independent fibers to form, the electrospinning jet must be allowed

time for most of the solvents to be evaporated. When the distance between the tip and the collector is reduced, the jet will have a shorter distance to travel before it reaches the collector plate. Moreover, the electric field strength will also increase at the same time and this will increase the acceleration of the jet to the collector. As a result, there may not have enough time for the solvents to evaporate when it hits the collector. When the distance is too low, excess solvent may cause the fibers to merge where they contact to form junctions resulting in inter and intra layer bonding as shown in Figure 2.5. This interconnected fiber mesh may provide additional strength to the resultant scaffold. Depending on the solution property, the effect of varying the distance may or may not have a significant effect on the fiber morphology.
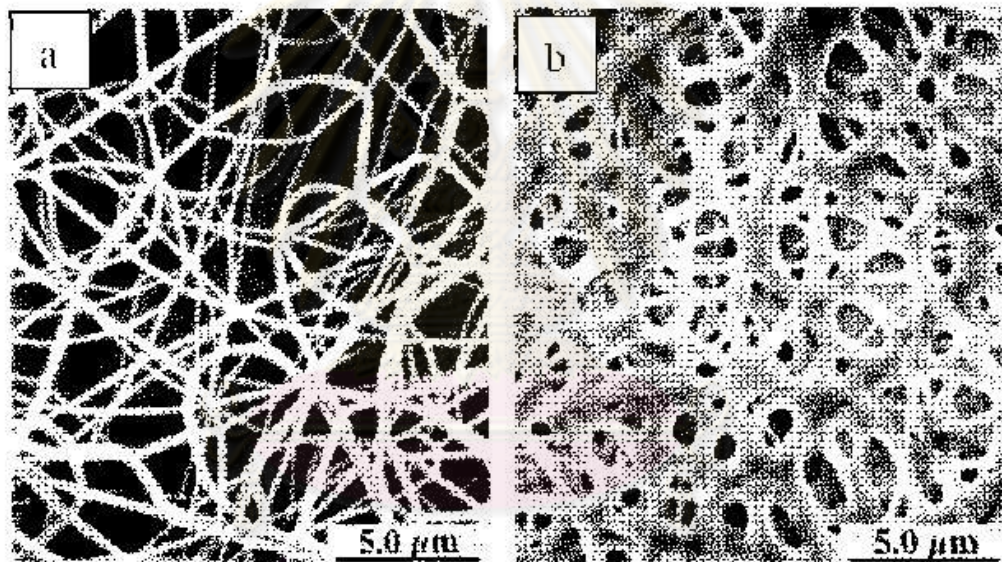
Figure 2.5 Nylon 6, 6 at (a) 2 cm deposition distance and (b) 0.5cm deposition distance [8].

The formation of beads may be the result of increased field strength between the needle tip and the collector. Decreasing the distance has the same effect as increasing the voltage supplied and this will cause an increased in the field strength. As mentioned earlier, if the field strength is too high, the increased instability of the jet may encourage beads formation. The longer distance means that there is a longer flight time for the solution to be stretched before it is deposited on the collector. However, there are cases where at a longer distance, the fiber diameter increases. This is due to the decrease in the electrostatic field strength resulting in less stretching of

the fibers. When the distance is too large, no fibers are deposited on the collector. Therefore, it seems that there is an optimal electrostatic field strength below which the stretching of the solution will decrease resulting in increased fiber diameters.

2.2.3 Environment parameters

The effect of the electrospinning jet surrounding is one area which is still poorly investigated. Any interaction between the surrounding and the polymer solution may have an effect on the electrospun fiber morphology. High humidity for example was found to cause the formation of pores on the surface of the fibers. Since electrospinning is influenced by external electric field, any changes in the electrospinning environment will also affect the electrospinning process.

2.2.1.3.1 Humidity

The humidity of the electrospinning environment may have an influence in the polymer solution during electrospinning. At high humidity, it is likely that water condenses on the surface of the fiber when electrospinning is carried out under normal atmosphere. As a result, this may have an influence on the fiber morphology especially polymer dissolved in volatile solvents. However, an increased in the humidity during electrospinning will cause circular pores to form on the fiber surfaces. The sizes of the circular pores increases with increasing humidity until they coalescence to form large, non-uniform shaped structures as shown in Figure 2.6. The depth of the pore also increases with increasing humidity as determined by atomic force microscopy.
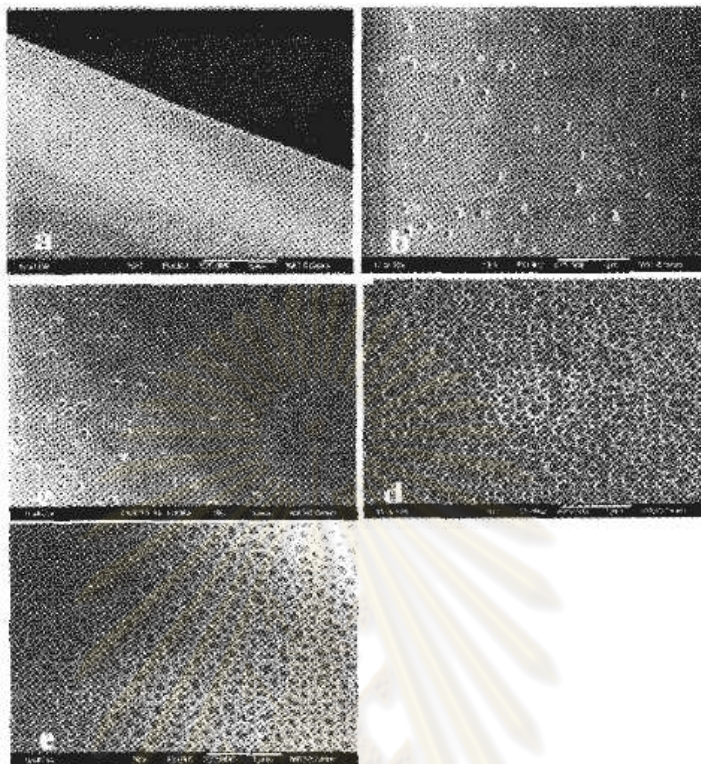
Figure 2.6 FESEM micrographs of 190 000 g/mol polysulfone/tetrahydrofuran fibers electrospun under varying humidity: (a) <25%, (b) 31-38%, (c) 40-45%, (d) 50-29%, (e) 60-72% [8].

The humidity of the environment will also determine the rate of evaporation of the solvent in the solution. At a very low humidity, a volatile solvent may dries very rapidly. The evaporation of the solvent may be faster than the removal of the solvent from the tip of the needle. As a result, the electrospinning process may only be carried out for a few minutes before the needle tip is clogged.

2.3 Fischer–Tropsch process

Since the invention of the original process by the German researchers Franz Fischer and Hans Tropsch, working at the Kaiser Wilhelm Institute in the 1920s, many refinements and adjustments have been made, and the term "Fischer-Tropsch" now applies to a wide variety of similar processes (Fischer-Tropsch synthesis or Fischer-Tropsch chemistry) [10].

The process was invented in petroleum-poor but coal-rich Germany in the 1920s, to produce liquid fuels. It was used by Germany and Japan during World War II to produce alternative fuels [11].

After the war, captured German scientists recruited in Operation Paperclip continued to work on synthetic fuels in the United States in a United States Bureau of Mines program initiated by the Synthetic Liquid Fuels Act. The Fischer-Tropsch process is a catalyzed chemical reaction in which carbon monoxide and hydrogen are converted into liquid hydrocarbons of various forms. Several reactions are required to obtain the gaseous reactants required for the Fischer-Tropsch catalysis.

The original Fischer-Tropsch process is described by the following chemical equation:

Fischer-Tropsch reaction

$$(2n+1)\ H_2 + n\ CO \rightarrow C_nH_{(2n+2)} + n\ H_2O \hspace{2cm} (2.4)$$

Water gas shift reaction

$$H_2O + CO \rightarrow H_2 + CO_2 \hspace{3cm} (2.5)$$

Synthesis gas formation

$$CH_n + O_2 \rightarrow \tfrac{1}{2}\ H_2 + CO \hspace{3cm} (2.6)$$
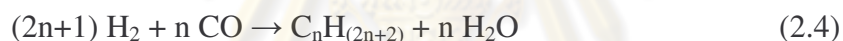
2.3.1 Fischer–Tropsch process conditions

a. Temperature 150-300°C (302-572°F).

b. Pressures 1-10 atm.

c. A variety of synthesis gas compositions can be used.

For Cobalt- based catalysts the optimal H_2:CO ratio is around 1.8-2.1. Iron-based catalysts promote the water-gas-shift reaction and thus can tolerate significantly lower ratios. This reactivity can be important for synthesis gas derived from coal or biomass which tend to have relatively low H_2:CO ratios (<1).

2.3.2 Primary reaction products

2.3.2.1 Low temperature Fischer–Tropsch reaction (< 250° C)

• Mainly normal paraffins (saturated, straight chain hydrocarbons - wax)

• Carbon number distribution determined by reaction condition, reactor
  type, reactant partial pressures, and catalyst

• Small amounts of olefins, alcohols, acids – catalyst dependent

• Most suitable for diesel fuel and synthetic lubricant product

2.3.2.2 High temperature Fischer–Tropsch reaction (> 300 ^{o}C)

• Mainly olefinic and aromatic hydrocarbons

• Very little heavier (wax) products, high C1-C3 gas yields

• Large amounts of oxygenated compounds

• Most suitable for gasoline and (commodity) chemical product

2.3.3 Reaction pathways in the Fischer-Tropsch synthesis

The Fischer-Tropsch synthesis is a polymerization reaction, in which the monomers are being produced from the gaseous reactants hydrogen and carbon monoxide. Thus, all reaction pathways proposed three different reactions [12].

      1. generation of the chain initiator

      2. chain growth or propagation

      3. chain growth termination or desorption

2.3.3.1 Alkyl mechanism

The alkyl mechanism is presently the most widely accept mechanism for chain growth shows the proposed reaction pathway for this mechanism. Chain initiation takes place via dissociative CO chemisortion, by which surface carbon and surface oxygen is generated. Surface oxygen is removed from the surface by reaction with adsorbed hydrogen yielding water or with adsorbed carbon monoxide yielding CO_2. Surface carbon is subsequently hydrogenated yielding in consecutive reaction CH,

CH$_2$ and CH$_3$ surface species. The CH$_3$ surface species is regarded as the chain initiator, and the CH$_2$ surface species as the monomer in this reaction. Chain growth is thought to take place by successive in corporation of the monomer, CH$_2$ surface species. Product formation take place by either β-hydrogen abstraction or hydrogen addition yielding α-olefins and n-paraffins as primary products. The surface species involved in the alkyl-mechanism have been found on the catalyst surface during the Fischer-Tropsch synthesis as shown as Figure 2.7.
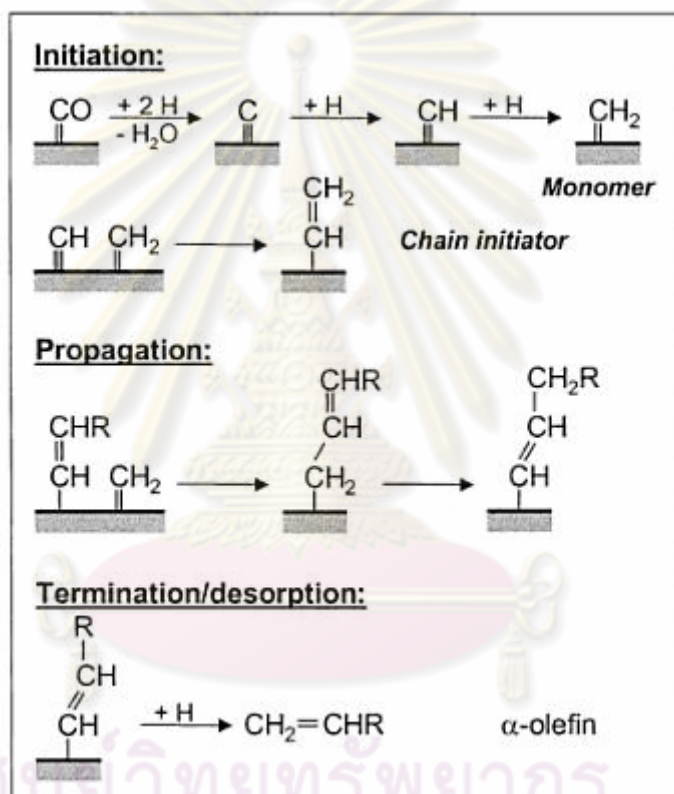
Figure 2.7 Alkyl mechanism [12].

2.3.4 Influence of process conditions on the selectivity

2.3.4.1 Temperature

An increase of temperature results in a shift toward products with a lower carbon number on iron, ruthenium, and cobalt catalysts as shown as table 2.1.

Table 2.1 Selectivity control in Fischer–Tropsch synthesis by process conditions and catalyst modifications [12].

Parameter	Chain length	Chain branching	Olefin selectivity	Alcohol selectivity	Carbon deposition	Methane selectivity
Temperature	↓	↑	*	↓	↑	↑
Pressure	↑	↓	*	↑	*	↓
H_2/CO	↓	↑	↓	↓	↓	↑
Conversion	*	*	↓	↓	↑	↑
Space velocity	*	*	↑	↑	*	↓
Alkali content iron catalyst	↑	↓	↑	↑	↑	↓

Note: Increase with increasing parameter: ↑. Decrease with increasing parameter: ↓. Complex relation: *.

2.3.4.2 Partial pressure of H_2 and CO

Most studies show that the product selectivity shifts to heavier products and to more oxygenate with increasing total pressure. Increasing H_2/CO ratios in the reactor result in lighter hydrocarbons and a lower olefin content. Increasing CO_2 pressures result in a decrease of the methane selectivity.

2.3.4.3 Catalyst

A variety of catalysts can be used for the Fischer–Tropsch process, but the most common are the transition metals cobalt, iron, and ruthenium. Nickel can also be used, but tends to favor methane formation (methanation) [13].

2.3.4.3.1 Cobalt based catalysts

Cobalt based catalysts are suited to produce high yields of long chain alkanes in Fischer–Tropsch synthesis [2]. Cobalt catalysts are a good choice for Fischer–Tropsch synthesis from natural gas derived synthesis gas and have a good balance between cost and stability. The water-gas shift activity of cobalt-based catalysts is low and water is the main oxygen containing reaction product. Cobalt-based catalysts are very suitable for wax formation in slurry bubble columns and can operate at high per pass conversion. Cobalt catalysts for Fischer-Tropsch synthesis of liquid and waxy paraffins from syngas were first discovered about 90 years ago. In the subsequent nine decades, catalyst technology has advanced from a simple cobalt oxide on asbestos to

sophisticated, high-activity, highly-optimized cobalt catalysts supported on carefully-modified alumina, silica, or titania carriers and promoted with noble metals and basic oxides. Catalyst design has evolved from trial and error art based on experimental reactor tests of activity and selectivity to a scientific, nanoscale design founded on activity-structure relationships and computerized theoretical models.

Important advances in cobalt catalyst design include:

a. Measurement of specific activities per site (turnover frequencies) based on H_2 uptake.

b. Development of methods for measuring metal dispersion, extent of reduction.

c. Development of activity-structure relationships, e.g. effects of preparation, pretreat-ment, dispersion, support properties, metal-support interactions, extent of reduction and promoters on catalyst activity and selectivity.

d. Development of a selectivity-transport model providing a quantitative relationship between selectivity and catalyst chemical and physical properties.

e. Development of stable, high-activity cobalt catalysts with high selectivities for liquid/wax products based on these activity structure relationships.

f. Optimization of catalyst performance based on the selectivity transport model.

2.3.4.3.2 SiO$_2$-supported Co catalysts

The textural properties of the support influence the catalytic activity and product selectivity of Co catalysts, via their modifications on the reducibility and dispersion of cobalt or the formation of well-fined phases. Synthesis of highly dispersed Co catalysts requires strong interaction between the support and the Co precursor, but in turn such strong interactions generally lower the reducibility of such precursors. Different from silica tend to have a strong interaction with cobalt precursor causing highly dispersed Co and limited reducibility [2]. Silica, as a common support used in the catalysts of Fischer-Tropsch synthesis, has the characteristics of a higher surface area, porosity, stability and weaker metal–support

interaction than aluminum as support. However, the weak interaction between cobalt and silica in silica-supported catalysts favors the reduction of cobalt precursor and promotes agglomeration of supported cobalt particles, reducing the dispersion of supported cobalt and the numbers of active sites [1].

Silica-supported cobalt catalysts in general exhibit high catalytic activities and liquid/wax hydrocarbon selectivities in Fischer-Tropsch synthesis of commercial significance. Several physical and chemical properties of silica make it an ideal support for Co Fischer-Tropsch synthesis catalysts. These include (1) its high surface area which favors moderately high Co dispersion at relatively high loadings of cobalt, and (2) its surface chemistry which enables high reduction of Co^{+3} or Co^{+2} to CoO[22].

2.4 Catalyst characterization

2.4.1 The morphology of catalysts

BET surface area and N_2 adsorption is used for determination of surface area of silica fiber.

Scanning electron microscope (SEM) is used for determination of the diameter of fiber and surface.

Transmission electron microscopy (TEM) is used for determination of shape and sizes of metal particles on the silica fiber.

2.4.2 Crystallization properties

X-ray diffraction (XRD) is used for determination of the orientation of a single crystal or grain, find the crystal structure material and measure the size, shape and internal stress of small crystalline regions.

2.4.3 Reducible properties

Temperature-programmed reduction (TPR) is used for determination of characterization of metal oxides, mixed metal oxides, and metal oxides dispersed on a support.

2.5 Literature review

In 2003 , Koski *et al.* [15] studied the molecular weight of polyvinylalcohol(PVA) and the solution concentration had a significant effect on the structure of the electrospun polymer which were produced by electrospinning technique. The solution was prepared by dissolving PVA with molecular weights ranging from 9000 to 186,000 g/mol in distilled water. After the PVA had dissolved completely, the solution was poured into the syringe. A voltage of 30 kV was applied to the solution, the collector was positioned at a distance of 102 mm from the needle and the solution jet emerging from the needle was collected on the aluminum foil. PVA had a degree of hydrolysis of 98–99%. The fiber obtained on the collector was examined by scanning electron microscopy.The results showed that the concentration of the polymer in the solution was varied depending on the molecular weight. The average fiber diameter was between 250 nm and 2 Am. The fiber diameter increases with MW and concentration. At low MW and/or concentrations, the fibers exhibit a circular cross-section. Flat fibers were observed at high MW and concentrations.

In 2003 , Shao *et al.* [16] prepared and studied the poly(vinyl alcohol) (PVA)/silica composite thin fibers which were produced by electrospinning in the diameter of 200-400 nm. A silica gels was varied silica content (0, 22, 34, 40, 49 and 59wt%) with the molar compositions of $TEOS:H_3PO_4:H_2O = 1:0.01:11$, was prepared by hydrolysis and polycondensation by dropwise addition of H_3PO_4 to TEOS with strong stirring at room temperature. After the above mixture reacted for 5 h, a certain amount of PVA solution of 10wt.% was dropped slowly into the silica gels, then reacted in a water bath at 60^oC for 12 h. The viscous solution of PVA/silica composites was contained in a plastic capillary. A voltage of 15–20 kV was applied to the solution and a dense web of fibers was collected on the aluminium foil. The obtained fiber mats were dried 12 h at 70^oC under vacuum. The fiber mats were characterized by IR, XRD, DSC, and TGA. The results indicated that PVA was changed from semicrystalline to amorphous state because of the increase of silica content. SEM photograph showed that junctions and bundles of the fiber mats decreased or almost disappeared, and bead increased with increasing silica content.

In 2003 , Guan *et al.* [17] prepared the PVA/cobalt acetate composite fibers which was produced by sol–gel processing and electrospinning technique in the diameter of 50–200 nm. PVA solution (about 10 wt.%) was prepared by dissolving PVA powder in distilled water and heating at $80^{\circ}C$ with stirring for 2 h, then cooling to room temperature and stirring for 12 h. Then, 20.0 g PVA solution of 10 wt.% was dropped slowly into the solution of cobalt acetate (1.0 g $Co(CH_3COO)_2 \cdot 4H_2O$ and 2.0 g H_2O), and the reaction proceeded in a water bath at $50^{\circ}C$ for 5 h. The viscous solution of PVA/cobalt acetate composites was contained in a plastic capillary. A voltage of 20 kV was applied to the solution and a dense web of fibers was collected on the aluminum foil. The fibers thus formed were dried initially 12 h at $70^{\circ}C$ under vacuum, and then calcined at $400–800^{\circ}C$ at 10 h. The fibers were characterized by SEM, FT-IR and WAXD. Results showed that the fiber after calcining the crystalline phase of Co_3O_4 appeared and morphology of the as-prepared fibers were largely influenced by the calcination temperature.

In 2004 , Siddheswaran *et al.* [18] prepared and studied the PVA/zinc acetate composite fibers which were produced by sol–gel processing and electrospinning technique in the diameter of 50–100 nm. PVA solution (about 10 wt%) was prepared by PVA (Mn 80,000) 20.0 g was dropped slowly into the solution of zinc acetate (1.5 g $Zn(CH_3COO)_2 \cdot H_2O$ and 2.0 g H_2O), and the reaction proceeded in a water bath at 60oC for 5 h. And, then it was contained in a plastic capillary. A voltage of 15 kV was applied to the solution and a dense web of fibers was collected on the aluminium foil. The fibers were dried at $70^{\circ}C$ for 8 h under vacuum and calcined at $700^{\circ}C$ for 5 h. The fibers were characterized by TG- DTA, SEM, FT-IR and XRD. Results showed that the fiber after calcining the crystalline phase of ZnO appeared.

In 2007 , Lihong *et al.* [19] studied the modification of SiO_2 by various organic groups such as methyltriethoxysilane (MTES), dimethyldiethoxysilane (DMDES), and chlorotrimethylsilane (TMCS), to change the surface silanol concentration on the SiO_2 support before the impregnation of cobalt. MTES modified SiO_2 (CH_3-SiO_2) was prepared by SiO_2 10 g was preheated at $200^{\circ}C$ for 12 h. Then cooled to room temperature under vacuum, and then transferred into a 250 ml conical

flask. After that 40 ml toluene and 5 ml MTES mixed in the conical flask and put into an ultrasonic bath (50 kHz) for 2 h at ambient temperature. The sample was then obtained by extracting with toluene in a Soxhlet extractor for 24 h and drying at 50ºC for 20 h under vacuum. The same method was used for the preparation of DMDES modified SiO_2 ((CH_3)$_2$-SiO_2) and TMCS modified SiO_2 ((CH_3)$_3$-SiO_2) using and, respectively. The Co catalysts (5 wt% cobalt loading) were prepared by impregnating CH3-SiO_2, (CH3)$_2$-SiO_2, and (CH3)$_3$-SiO_2 with ethanol solutions of cobalt nitrate. The samples were dried at 120ºC and calcined in air at 600ºC for 6 h. Co/SiO_2 catalyst was used as a reference. These were characterized by IR, XRD, and TPR. Results showed that the organic modification of SiO_2 reduced the surface silanol (Si–OH) concentration of the SiO_2 support, suppressed the interaction between cobalt and silica, enhanced the reduction of the supported cobalt, and thus increased the catalytic activity of Co catalysts for Fischer–Tropsch synthesis. Moreover, SiO_2 modified by different organic groups had different surface silanol concentration because of the steric hindrance, and the catalytic activity increased with the decrease of surface silanol concentration.

In 2008 , Hinchiranan *et al.* [2] studied the addition of small amount of TiO_2 to silica/cobalt catalysts for Fischer–Tropsch synthesis. The titania-modified silica supports were prepared by incipient wetness impregnation. After impregnation, the samples were dried at 393 K for 12 h, and then calcined at 673 K for 2 h. The loading amount of TiO_2 was 2, 5 and 10wt%, respectively. The properties of various catalysts were characterized by in-situ DRIFT, XRD, TPR, N_2 physisorption and H_2 chemisorption. The catalysts were reduced with H_2 at 673 K for 10 h followed by passivation with 1% O_2 in N_2. The Fischer–Tropsch synthesis conditions were P (total) = 1.0 MPa, T = 513 K, CO / H_2 = 1 / 2, W / F (CO+H_2+Ar) = 5 g cat h mol^{-1}. Results showed that the increasing in amounts of TiO_2 to silica-supported cobalt catalysts, the increasing in the dispersion of cobalt and Co metallic surface area. The addition of TiO_2 adjusted the interaction between cobalt and silica support quite well to realize the favorite dispersion and reduction degree of supported cobalt, leading to high catalytic activity in Fischer–Tropsch synthesis.

In 2006 , Wan *et al.* [20] studied the effect of adding SiO_2 to a precipitated iron-based Fischer–Tropsch synthesis (FTS) catalyst. Two catalysts were prepared by co-precipitated and spray-dried method. A solution containing both $Fe(NO_3)_3$ and $Cu(NO_3)_2$ with a weight ratio of 100Fe / 6Cu was precipitated at 80^oC using Na_2CO_3 solution. After precipitation and filtration, the precipitate was divided into two parts: one of them was added with K_2CO_3 solution and silica gel in amounts required to obtain the desired weight ratio of 100Fe / 5K / $25SiO_2$. The other part of precipitate was only added with the appropriate amount of K_2CO_3 solution to obtain an unsupported iron-based catalyst. The slurry was spray dried and then was calcined at 450 ∘C for 5 h. The calcined catalyst was crushed and sieved to obtain 20–40 mesh for reaction. These were characterized by N_2 physical adsorption, H_2 differential thermogravimetric analysis, temperature-programmed reduction/desorption (TPR / TPD) and Mossbauer spectroscopy. The Fischer–Tropsch synthesis conditions were 260∘C, 2.0MPa, H_2 / CO = 2.0 and GHSV= $1000h^{-1}$. Incorporation of SiO_2 to precipitated iron-based catalyst was found to have significant influences on the surface basicity, reduction and carburization behaviors, as well as catalytic activity. The changes in the catalytic performances can be primarily attributed to the effects of SiO_2 on the Fe / Cu and Fe / K contacts, which lead to different degrees of H_2 and CO adsorption and further significantly affect the FTS performances of the catalyst. SiO_2 stabilizes the iron oxide crystallites from sintering, facilitates the high dispersion of Fe_2O_3 and CuO and further enhances the contact between Fe_2O_3 and CuO. The enhanced Fe/Cu contact enhances the ability of H_2 adsorption and promotes the reduction of $Fe_2O_3{\rightarrow}FeO_x$, while the transformation of $FeO_x{\rightarrow}Fe$ is suppressed due to the stronger Fe–SiO_2 interaction. Furthermore, due to the strong Fe–SiO_2 and K–SiO_2 interactions, catalyst incorporated with SiO_2 has weak contact between Fe and K, which weakens the surface basicity of the catalyst and severely suppresses the carburization, resulting in the weak CO adsorption. In the FTS reaction, the FTS activity is decreased by the addition of SiO_2 due to the weak carburization, whereas SiO_2 could suppress carbon deposition and thus improves the catalyst stability. With incorporation of SiO_2, the hydrocarbon selectivity was strongly affected. The product distribution shifts to the light hydrocarbons and the olefin selectivity in total product

decreases on the catalyst due to the surface basicity weakened indirectly by the addition of SiO_2.

In 2006 , Song *et al.* [21] studied the effect of catalyst pore size on the catalytic performance of silica supported cobalt Fischer–Tropsch catalysts. A series of cobalt catalysts supported on silica with different pore size were prepared by incipient wetness impregnation method. The samples were impregnated with the appropriate $Co(NO_3)_2.6H_2O$ solution, then dried at 383K for 12 h. Finally, the catalyst precursor was calcined in air at 673K for 6 h. All the Co/SiO_2 catalysts contain 15 wt% cobalt. These were characterized by N_2 physisorption, XRD, H_2-TPR, H_2-TPD, DRIFTS and O_2 pulse reoxidation. The Fischer–Tropsch synthesis conditions were H_2/CO (mol%) = 2, T = 503∘C and P(total) = 10 bar. Results showed the pore size of the support had a significant influence on the Co_3O_4 crystallite diameter, catalyst reducibility and Fischer–Tropsch activity. The larger pore could cause the Co/SiO_2 to form larger Co_3O_4 crystallite and decreased its dispersion. Catalysts with different pore size showed different CO adsorption property. The catalysts with pore size of 6–10 nm displayed higher Fischer–Tropsch activity and higher C_{5+} selectivity, due to the moderate particle size and moderate CO adsorption on the catalysts.

In 2009 , Bae *et al.* [22] studied the Cobalt supported on amorphous aluminum phosphate (Co / $AlPO_4$) catalysts were prepared by the impregnation method using three different cobalt precursors such as cobalt nitrate, acetate and chloride to elucidate the activity of Fischer–Tropsch synthesis. Amorphous aluminum phosphate with a P / Al ratio of 0.9 was prepared from $Al(NO_3)_3.6H_2O$ and $(NH_4)_2HPO_4$. The starting materials were dissolved in deionized water (400 mL of 0.5 M of Al nitrate solution and 350ml of 0.5M of $(NH_4)_2HPO_4$ solution) and acidified with nitric acid. A hydrogel was formed by adding 700ml of 10% solution of ammonia to the acidified solutions of Al and P precursors until a pH of 8.0. After 1 h, the contents were filtered and the hydrogel was washed with twice its volume of distilled water. The hydrogel was dried at 110^oC for 16 h and calcined at 500^oC in air for 0.5 h. The Fischer–Tropsch synthesis conditions were T = $220–240^oC$, P = 2.0MPa, SV (1 / kgcat / h) = 2000 and H_2 / CO / CO_2 / Ar (mol%) = 57.3 / 28.4/ 9.3/

5.0. These were characterized by XRD, TPR, FT-IR and DRIFT, XPS, TEM and Ramanand chemisorption analysis. The Co/AlPO$_4$ catalysts prepared from cobalt nitrate precursor show higher CO conversion and C$_{8+}$ selectivity than the catalysts prepared from the corresponding precursors such as acetate and chloride due to the facile reduction properties with a proper electronic state of reduced cobalt species and large pore diameter with the diffusion-enhanced re-adsorption of α-olefins. The higher selectivity of C$_{8+}$ was found to be in the order of CoN > CoA > CoCl catalyst. Interestingly, all Co/AlPO$_4$ catalysts compared with Co/Al$_2$O$_3$ catalyst. The differences in the catalytic properties exhibited by Co/AlPO$_4$ catalysts were attributed to the cobalt particle size, reducibility with different electronic states of cobalt species which was enhanced the dissociative adsorption of CO molecule (linear- and bridged-type CO species) and a large pore size of AlPO$_4$ with a facile diffusion of formed hydrocarbons as well as filamentous carbon formation.

CHAPTER III

EXPERIMENTAL

3.1 Materials

All Chemicals used in this experiment were listed in table 3.1.

Table 3.1 List of chemicals and sources

Chemicals	Source
Tetraethyl orthosilicate ($C_8H_{20}O_4Si$) 98.0%	Fluka
Hydrochloric acid 37.0%	CARLO ERBA
Ethanol 99.8%	Analar Nor Mapur
Polyvinylpyrrolidone	Fluka
Cobalt(II) acetate ($CH_3COO)_2Co.4H_2O$	Fluka
Glycerol ($C_3H_8O_3$) 99.5%	Univar
Silica supports 5-10 mesh	Fuji Silysia
Nitrogen gas (99.99% purity)	Praxair
Hydrogen gas (99.99% purity)	Praxair
Carbon monoxide gas/Hydrogen gas (CO/H_2) 1:2	BOC Scientific
Helium gas (99.99% purity)	Praxair
Standard synthesis gas 20% of CO 20% of CH_4 and 20% H_2 bal He	BOC Scientific
Standard synthesis gas 100% of CO_2	Praxair

3.2 Instruments and equipments

    3.2.1 Instruments and equipment for catalyst preparation

        1. High voltage power supply

        2. Syringe pump

        3. Ultrasonic bath

        4. Water bath

5. Hot plate

6. Oven

7. Mechanical stirrer and impeller

8. Magnetic stirrer

9. Pipette 5 and 10 mL

10. Thermometer

11. Beaker 50, 100 and 250 mL

12. Inject bottle

13. Stirring rod

14. Dropper

15. Spoon

16. Disposal syringe

17. Dessicator

18. Aluminium foil

19. Stainless steel screen 20 x 20 cm

20. Needle (inner diameter 0.6 and 0.4 mm)

21. Crucible

3.2.2 Instruments and equipment for catalyst characterization

1. BET (Micromeritics ASAP 2020)

2. Scanning electron microscope (SEM) (JOEL model JSM-6480LV)

3. Energy dispersive spectroscope (EDS)

4. X-ray diffractometer (XRD) (Philips model X'Pert)

5. Temperature programmed reduction (TPR) (GC) (Shimadzu GC-2014)

6. Transmission electron microscope (TEM) (JEOL model JEM-1230)

3.2.3 Instruments and equipment for Fischer-Tropsch process

1. Fixed bed reactor

2. Tube furnace

3. Temperature controller

4. Mass flow rate

5. Thermocouple

6. Gas Chromatograph (GC) (Shimadzu GC-2014)

3.3 Preparation and characterization of catalyst

3.3.1 Preparation of polymer solution

The polymer solution was prepared from poly(vinyl-pyrolidone) (PVP) and ethanol. The ratio of PVP:ethanol (g/g) was 0.5:5, 1:5, 1.5:5, 2:5, 2.5:5, 3:5, 4:5, 5:5, 6:5, and 7:5. PVP and ethanol was pre-mixed at the given ratios under stirring for 10 min [18].

3.3.2 Sol-Gel preparation

A silica sol was prepared from tetraethyl orthosilicate (TEOS), ethanol, distillated water and HCl. The molar ratio of TEOS:ethanol:H_2O:HCl was 1:2:2:0.01. TEOS and H_2O were mixed and stirred for 5 min, added conc.HCl and stirred for 5 min. Also added EtOH and stirred for 5 min. Then stirred the solution on water bath at 55^oC for 35 min. Finally slowly added polymer solution into the solution and stirring for 5 min [16].

3.3.3 Electrospinning condition

In this research, 2 parameters in electrospinning technique such a needle size and polymer solution were studied. The parameters were varied as follow: needle size; 0.6 and 0. 4 mm (inner diameter) and polymer solution (PVP):EtOH ratio; 10 20 30 40 50 60 and 70wt%. TCD and voltage were fixed at 15 cm and 15 kV. The electrospun fibers were collected on aluminum foil. After that fibers were calcined at 600^oC for 2 h.
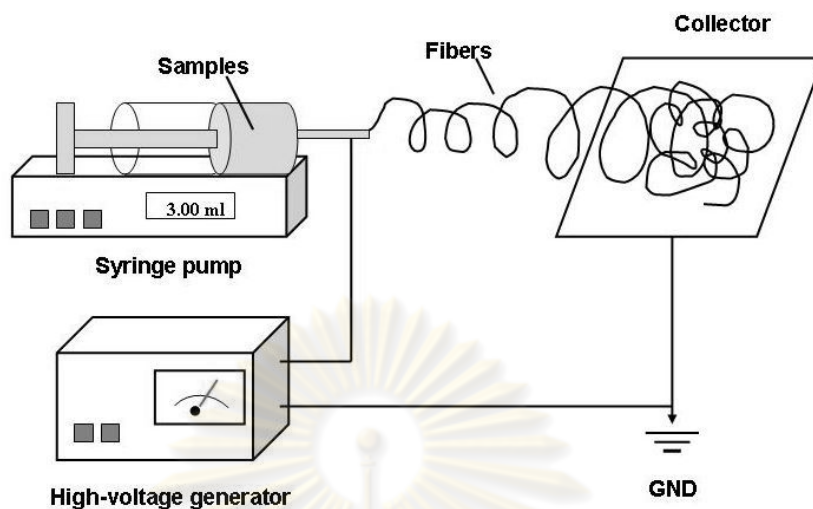
Figure 3.1 The electrospinning process apparatus.

3.3.4 The influence of the parameters on the electrospinning process

The effect of the parameters on the fiber diameter and morphology were investigated, and were listed as follows:

       1. The effect of needle size (0.6 and 0.4 mm)

       2. The effect of voltage (15, 20 and 25 kV)

       3. The effect of tip to collector distance (15 and 20 cm)

       4. The effect of polymer amount (5, 10, 20, 30, 40, 50, 60 and 70 wt% PVP)

3.3.5 Impregnation

The cobalt/silica was prepared by impregnation method. The prepared fibers were impregnated with the various percent loadings of cobalt nitrate solution. Then dried at 110°C for 12 h. Finally, the catalyst was calcined at 600°C for 2 h. All the cobalt/silica catalysts contained 5, 10, 15 and 20 wt% cobalt.

3.3.6 Characterization of fiber catalyst

3.3.6.1 BET surface area

BET surface area and N_2 adsorption at 60^oK (The Micromeritics ASAP 2020) was used to determine surface area of silica fiber.

3.3.6.2 Scanning electron microscope (SEM)

Scanning electron microscope (SEM) was used to research morphology and average diameter of fiber, used a Scanning electron microscope (SEM) (JOEL model JSM-6480LV). The composition of fiber determined by EDS. The size of fiber was determined using a SemAfore program.

3.3.6.3 Temperature program reduction (TPR)

Temperature programmed reduction (TPR) was used to determine the reduction behavior of catalysts. 0.1 g of catalysts was heat from room temperature to 100^oC with the heating rate of $10^oC/min$, and kept for 30 min. After that was passed N_2 to remove the adsorbed water and other impurity. The reducing gas containing 5% H_2 in N_2 was passed over the catalyst at a flow rate 30 mL/min with the heating rate of $3^oC/min$ up to 600^oC as shown in figure 3.2.

Determination of percentage of cobalt reduction of catalyst was calculated as follows:

$$\text{Reduction degree (\%)} = 100 \times \frac{\text{mole of } H_2 \text{ consumption }_{measured}}{\text{mole of } H_2 \text{ consumption }_{calculated}}$$
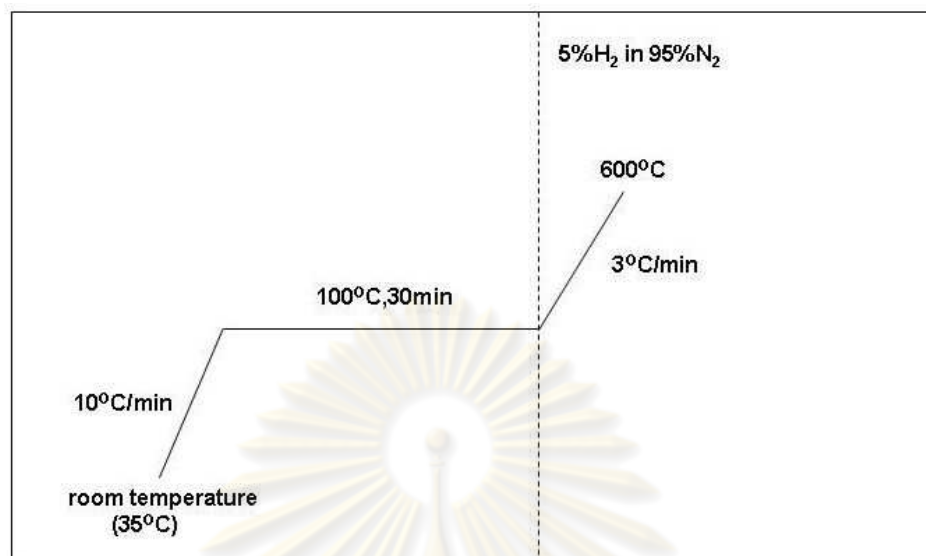
Figure 3.2 Schematic of temperature program reduction reaction.

3.3.6.4 X-ray diffraction (XRD)

X-ray diffraction was used to determine the structure and crystallite size of out The Philips model X'Pert diffractometer was used with Cu Kα radiation. The catalyst for XRD measurement was at an angle of 2θ ranged from 20 from 70 degrees.

3.4 Fischer-Tropsch process

3.4.1 Reaction procedure

1. Packed 0.2 g of cobalt/silica fiber catalyst into the middle of the fixed bed quartz reactor.

2. Set temperature of tube furnace to $400^{o}C$ for reduction of catalyst with hydrogen gas (flow rate = 30 ml/min) under atmospheric pressure for 3 h and then switch into nitrogen gas (flow rate = 20 mL/min).

3. Set temperature of tube furnace at 260, 280 and $300^{o}C$.

4. Flowed CO/H$_2$ ratio 2:1 (flow rate = 15 mL/min).

5. After 10 min of the reaction, the produced gas was analyzed by gas chromatography of which the optimum condition was shown in table 3.2.

Table 3.2 The optimum condition of gas chromatography.

Carrier gas	He 99.999%
Column	Unibead C
Injector temperature	120^oC
Column temperature	Temperature program
	80^oC 3min
	180^oC (20^oC/min)
	180^oC 8min
Detector temperature	200^oC
Detector	Thermal conduct detector (TCD)
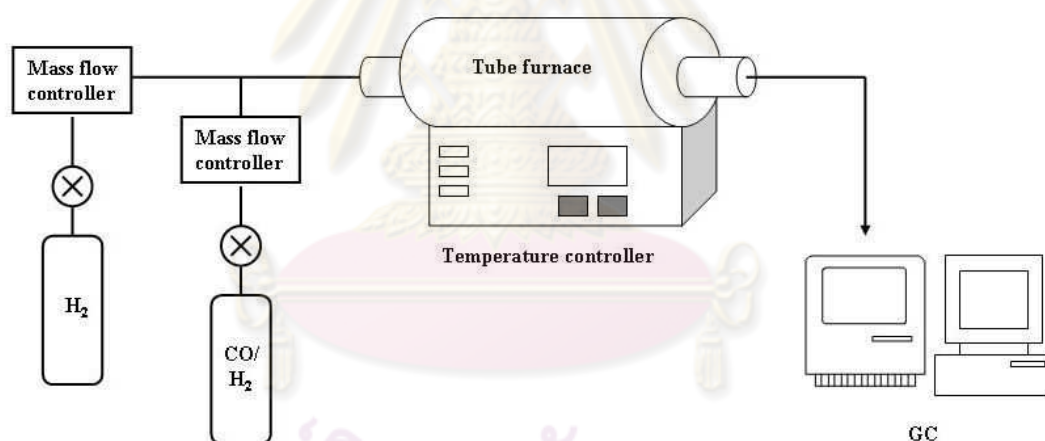
Figure 3.3 Flow diagram of Fischer-tropsch process.

3.5 The influence of the operating parameters on the Fischer-Tropsch reaction

      1. The effect of support (porous and fiber)

      2. The effect of reaction temperature (260, 280 and 300^oC)

      3. The effect of Cobalt loading in catalyst (5, 10, 15 and 20 wt%)

CHAPTER IV

RESULTS AND DISCUSSION

4.1 Catalyst preparation

4.1.1 The effect of needle size

The effect of needle size on electrospun fiber was investigated by fixing the collector distance and voltage at 15 cm and 15 kV, respectively. The SEM results of the electrospun fibers were shown in figure 4.1(a) (b) (c) (d) and (e) and 4.2 (a) (b) (c) (d) (e) and (f), respectively. The SEM results showed that the fiber diameters were in submicron after calcined at 600°C for 2 h (Table 4.1). The average diameter of electrospun fiber was depended on the needle size. The larger the needle size, the bigger the electrospun fiber diameter. The electrospinning process with needle size 0.4 mm was appropriate condition to produce the smallest fiber with the balance on the voltage and surface tension of the electrospinning solution, in this experiment. The average diameter of fibers obtained by needle size at 0.4 mm was 0.820 μm. As shown in results, needle size decreased let to an increasing of surface tension of droplets. For the same applied voltage, a greater columbic force was required to cause jet initiation. Results indicated that the decreasing acceleration of jet gave a long time for solution to be stretched and elongated before it was collected so the fiber was small [8].

4.1.2 The effect of PVP content

The effect of PVP content on electrospun fiber was investigated by fixing the collector distance, voltage and needle size at 15 cm, 15 kV and 0.4 mm, respectively. The SEM results of the electrospun fibers were shown in figure 4.2(a) (b) (c) (d) (e) and (f), respectively. The SEM results showed that the fiber diameters were in submicron after calcined at 600°C for 2 h (Table 4.1). Electrospun fiber before and after calcining have smooth surface area and the diameter of electrospun fiber after calcining was smaller than before calcining. Due to the removal of PVP, the average

diameter of electrospun fiber was depended on the PVP content [18]. The more PVP content, the smaller the electrospun fiber diameter. The average diameter of fibers using PVP content at 70 wt% was 0.448 μm. When PVP content was more than 70 wt%, the electrospun fiber could not be prepared by electrospinning process because PVP powder could not be soluble in ethanol.
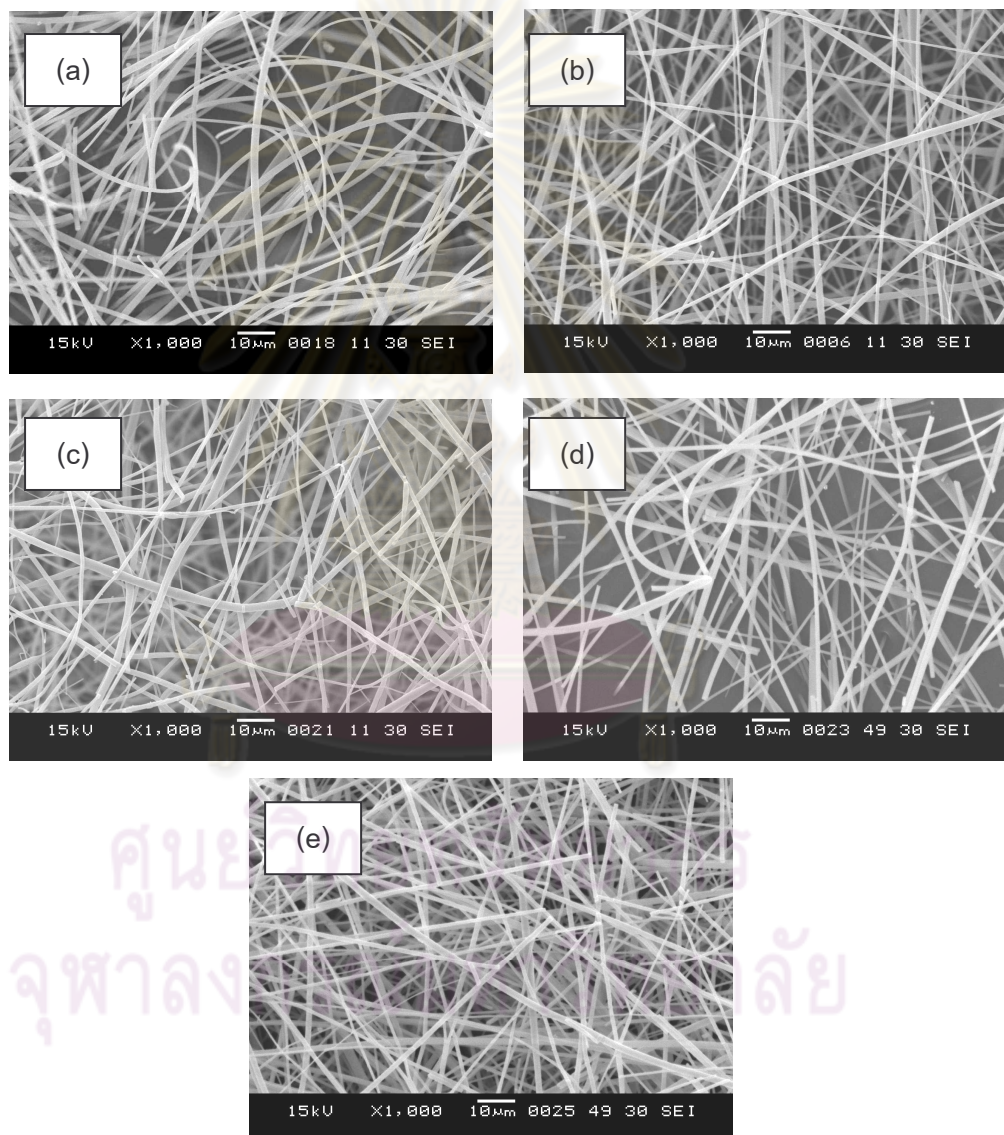
Figure 4.1 The SEM results of fibers calcined at 600°C for 2 h with various PVP content, (a) 5 wt%, (b) 10 wt%, (c) 15 wt%, (d) 20 wt%, and (e) 25 wt%. The tip to collector distance was 15 cm, voltage was 15 kV and needle size was 0.6 mm.
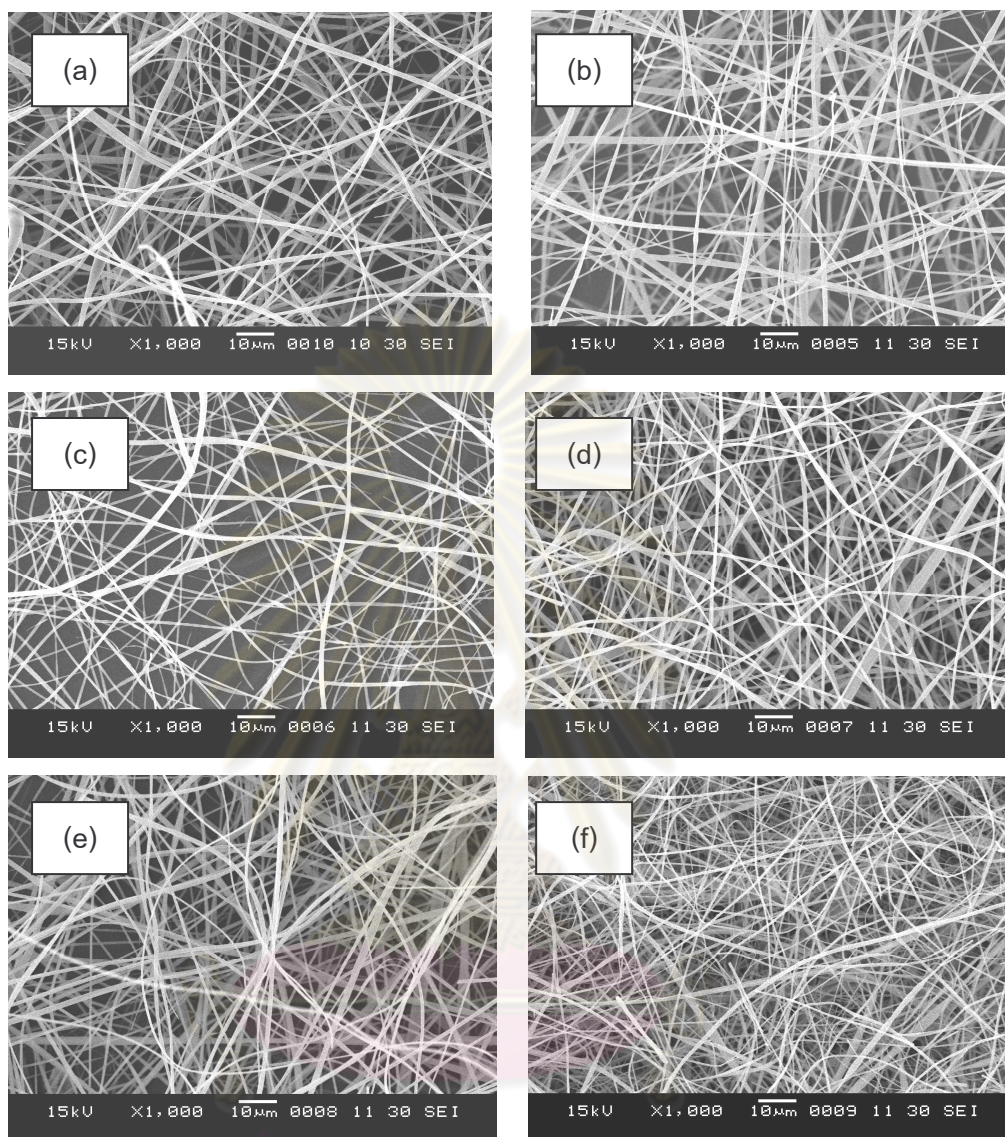
Figure 4.2 The SEM results of fibers calcined at 600°C for 2 h with various PVP content. (a) 25 wt%, (b) 30 wt%, (c) 40 wt%, (d) 50 wt%, (e) 60 wt%, and (f) 70 wt%. The tip to collector distance was 15 cm, voltage was 15 kV and needle size was 0.4 mm.

Table 4.1 The average diameter of fibers with various needle size and   PVP content,TCD = 15 cm and applied voltage = 15 kV.

PVP:EtOH (wt.%)	Needle size (mm)	
	0.6	**0.4**
	Average diameter (μm)	
5	2.105	-
10	1.867	-
15	1.782	-
50	1.785	-
25	1.612	0.820
30	-	0.713
40	-	0.685
50	-	0.659
60	-	0.515
70	-	0.468

4.1.3 The effect of applied voltage

The effect of applied voltage on electrospun fiber was investigated by fixing the collector distance, needle size and PVP content at 15 cm, 0.4 mm and 70 wt%, respectively. The SEM results of the electrospun fibers were shown in figure 4.3(a) (b) and (c), respectively. The SEM results showed that the fiber diameters were in submicron after calcined at 600°C for 2 h (Table 4.2). The average diameter of electrospun fiber using 20 kV was 0.448 μm that was smaller than using 15 and 25 kV. Due to the increasing in applied voltage, the amounts of charges were increased. An increase of the columbic repulsive force in the jet, let to an increase of acceleration and the drawing of the solution to the collection plate which was faster than the supply from the source. Thus the Taylor cone may recede into the needle resulting in smaller and less stable initiated jet. When the applied voltage was too high, the acceleration of the fiber was increased. This reduction of the flight time of

the electrospinning jet thus the fiber was large [8]. The distribution diameter of electrospun fibers using voltages 15, 20 and 25 kV was shown in figure 4.4(a) (b) and (c), respectively. The distribution diameter of fiber at 20 kV was only 400-600 nm while the distribution diameter of fiber at 25 kV were found to be 400--800 and >1000 nm.
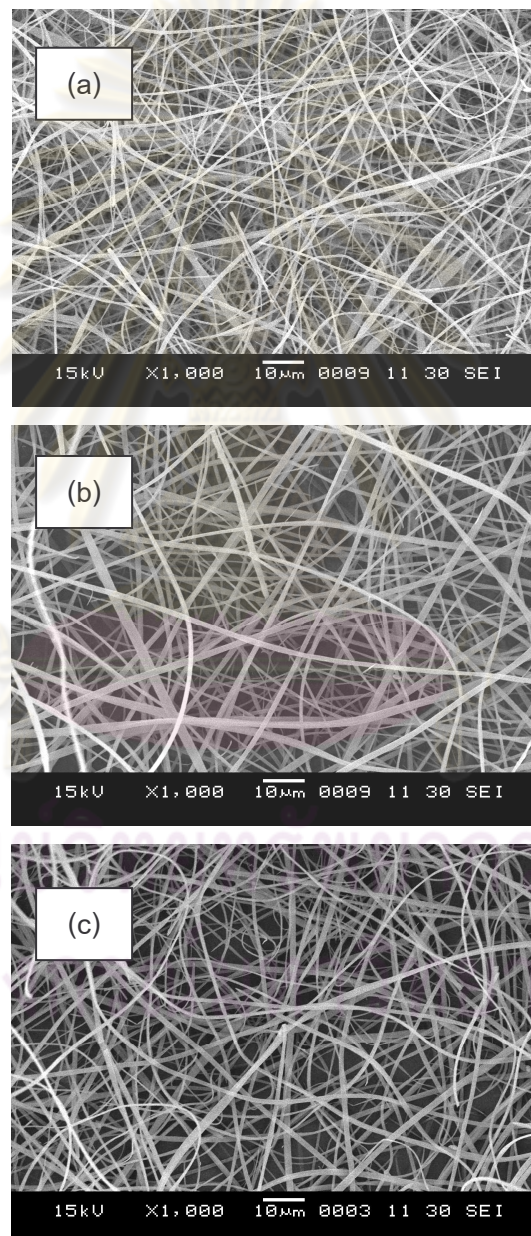
Figure 4.3 The SEM results of fibers calcined at 600°C for 2 h with various voltages (a) 15 kV, (b) 20 kV, and (c) 25 kV. Needle size was 0.4 mm, PVP content was 70 wt% and the tip to collector distance was 15 cm.
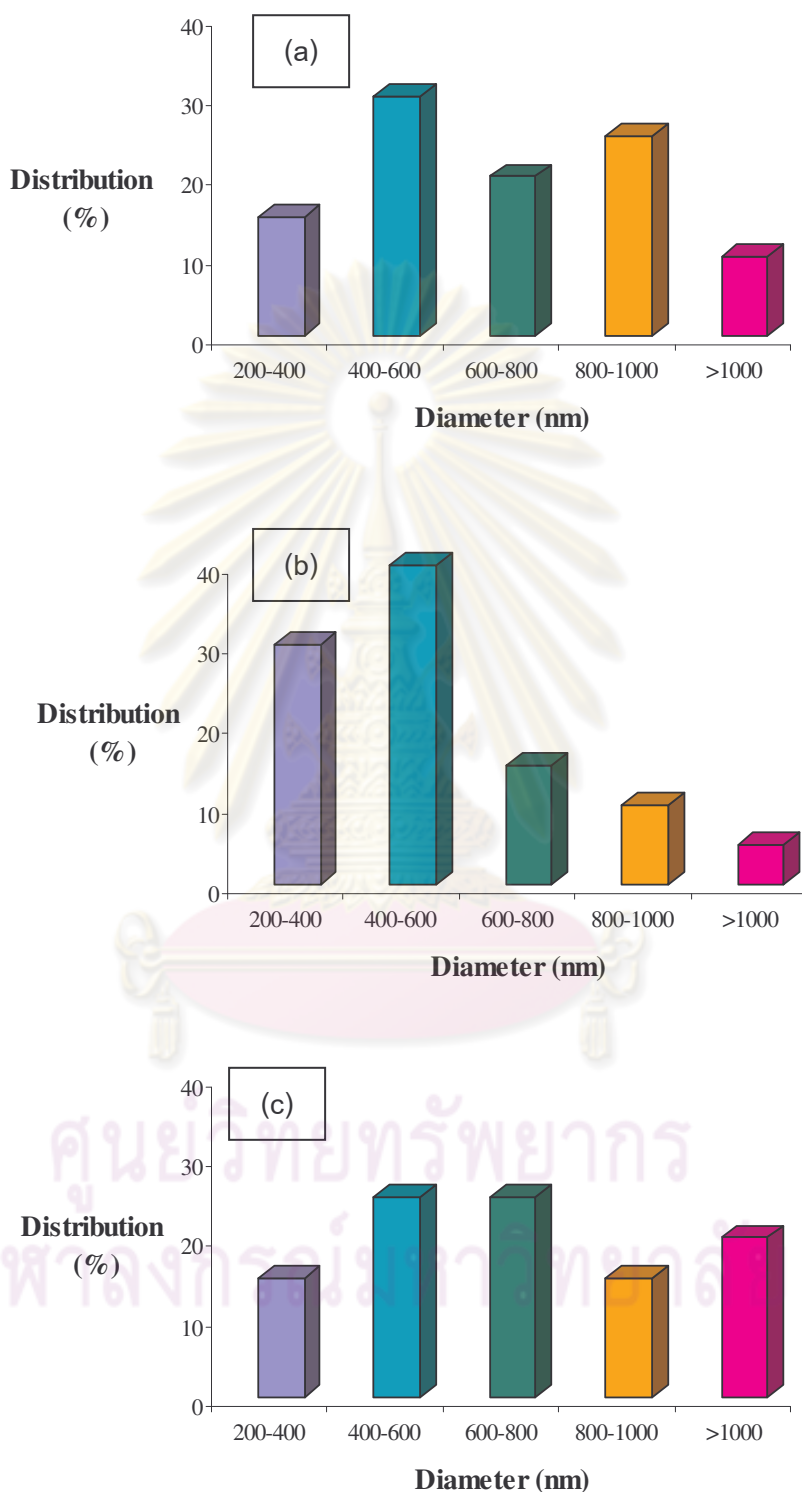
Figure 4.4 Diameter distribution of fibers calcined at 600°C for 2 h at different voltage. (a) 15 kV, (b) 20 kV, (c) 25 kV. Needle size was 0.4 mm, PVP content was 70 wt% and the tip to collector distance was 15 cm.

4.1.4 The effect of the tip to collector distance (TCD)

The effect of the tip to collector distance on electrospun fiber was investigated by fixing voltage, needle size and PVP content at 20 kV, 0.4 mm and 70 wt%, respectively. The SEM results of the electrospun fibers were shown in figure 4.5(a) and (b), respectively. The SEM results showed that the fiber diameters were in submicron after calcined at 600°C for 2 h (Table 4.2). The average diameter of electrospun fiber using tip to collector distance 15 cm was 0.448 μm that was smaller than using tip to collector distance 20 cm. The distance between the tip and the collector might have influenced that in the flight time and the electric field strength. An increase of distance between tip and collector, results in an increment of in diameter of fiber. When the distance was too long, no fibers were deposited on the collector. At 20 cm distance, the decreasing in electrostatic field strength and the decreasing in acceleration of the jet to collector were found let to an increase size of fiber [8]. In table 4.2, the average diameter of fibers obtained by 20 cm and applied voltage 25 kV was 1.180 μm. In addition the tip to collector distance and voltage was 20 cm and 25 kV leading to increasing in the electrostatic field strength and the increasing in acceleration of the jet to collector thus this reduced the flight time of the electrospinning jet thus the fiber was larger.
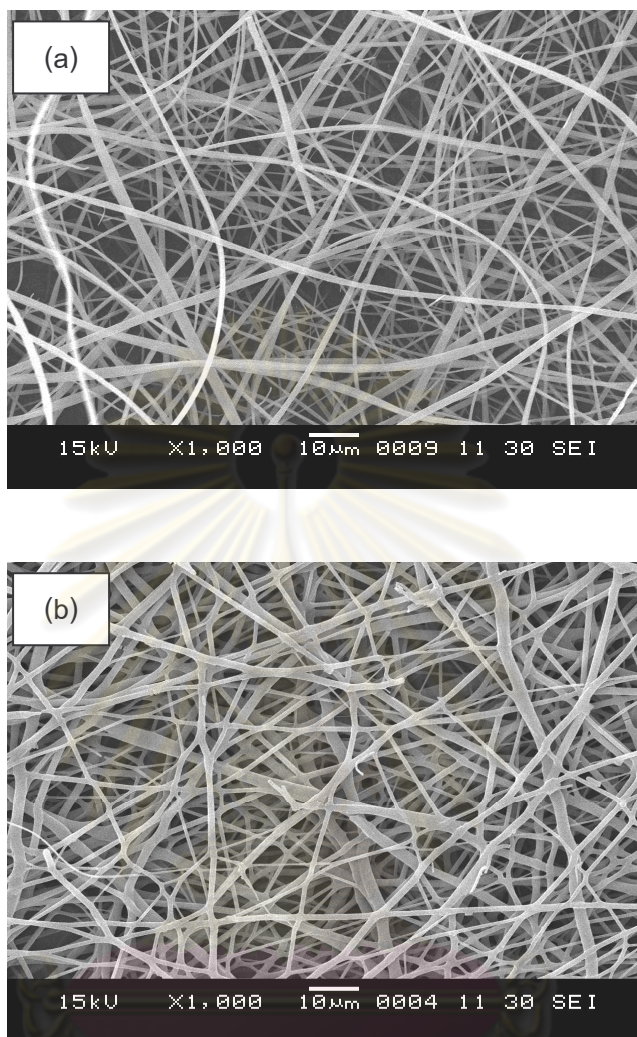
Figure 4.5 The SEM results of fibers calcined at 600°C for 2 h with various the tip to collector distance (a) 15 cm (b) 20 cm. Needle size was 0.4 mm, PVP content was 70 wt% and voltage was 20 kV.

Table 4.2 The average diameter of fibers with various TCD = 15 and 20 cm and applied voltage = 15, 20 and 25 kV. Needle size = 0.4 mm and PVP content = 70 wt%.

TCD (cm)	Voltage (kV)	Average diameter (mm)
15	15	0.468
15	20	0.448
15	25	0.674
20	15	0.625
20	20	0.601
20	25	1.180

The comparison of surface area between porous silica and silica fiber was shown in table 4.3. The surface area of porous silica was measured by BET method and the surface area of silica fiber was calculated by the mathematic calculation from the SEM photograph because silica fiber could not be analyzed by BET. Results were shown in figure 4.7, the adsorption and desorption properties of silica fiber could not determined because silica fiber had no pore. Table 4.3 showed the BET result that the porous silica had the surface area of $237.36 m^2/g$ and the silica fiber had the surface area of $2.76 m^2/g$.

Figure 4.6 displayed the adsorption isotherm of mesoporous silica. The adsorption isotherm type V, that the hysteresis loop was created by the capillary condensation of the adsorbate in mesopores of the silica solid, described the monolayer and multilayer adsorption plus capillary condensation properties [23].

Table 4.3 The surface area of silica porous and silica fiber photograph.

BET result	Silica Porous	Silica Fiber
Surface area (m^2/g)	237.36	2.76
Pore volume (cm^3/g)	1.01	N/A
Pore size (nm)	16.9	N/A

*Surface area = 2 / (SiO_2density (g/cm^3) × radius fiber (µm)) (Mathematic calculation)
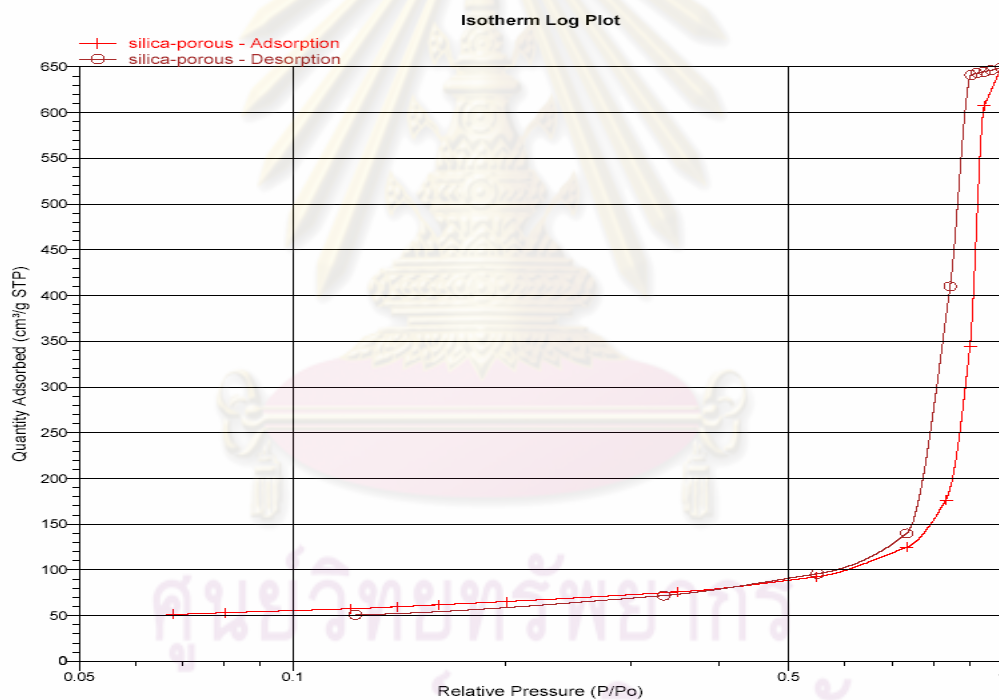
Figure 4.6 The N_2 adsorption isotherm of silica porous support.
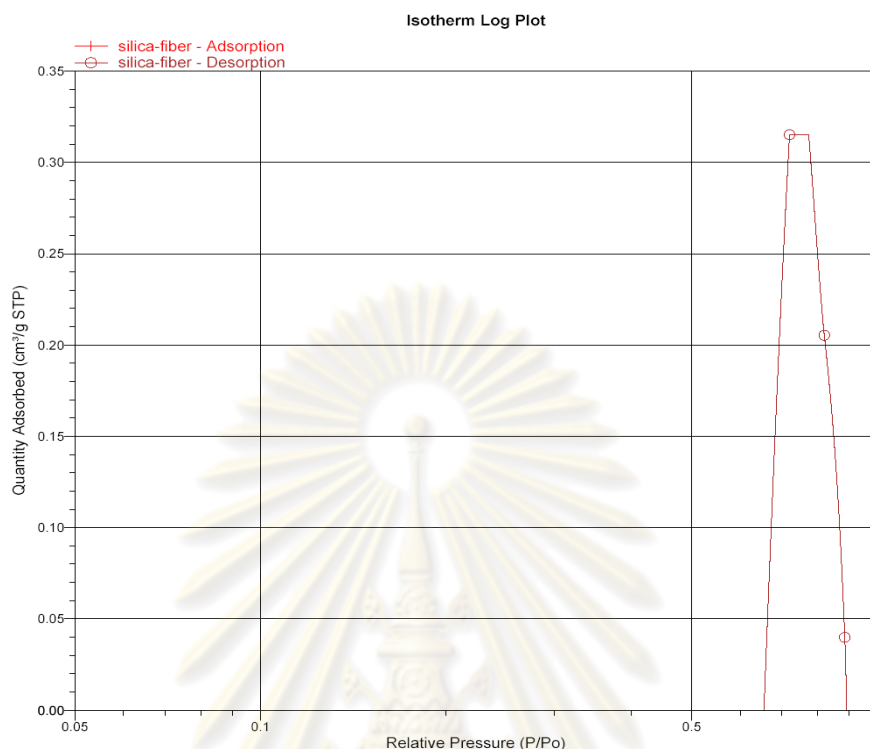
Figure 4.7 The N_2 adsorption isotherm of silica fiber support.

4.1.4 The effect of cobalt content.

The effect of cobalt content on electrospun fibers was investigated by varying cobalt content at 5, 10, 15 and 20 wt%. Fiber catalyst was prepared by cobalt impregnation method. The morphology of Co/SiO_2 fiber catalysts analyzed by SEM at the 50,000 times magnification. The SEM results were shown in figure 4.8(a) (b) (c) and (d), respectively. The SEM results were showed that the surface of Co/SiO_2 fiber catalyst was rough because cobalt particles dispersed over the silica fibers. The surface of the higher cobalt content was rougher than the lower cobalt content. Results were indicated that cobalt particles of the high cobalt content were larger than the low cobalt content. Fifteen and twenty wt% cobalt content impregnated with silica fiber, the clusters of cobalt particles were observed (figure 4.8 (c) and (d)).
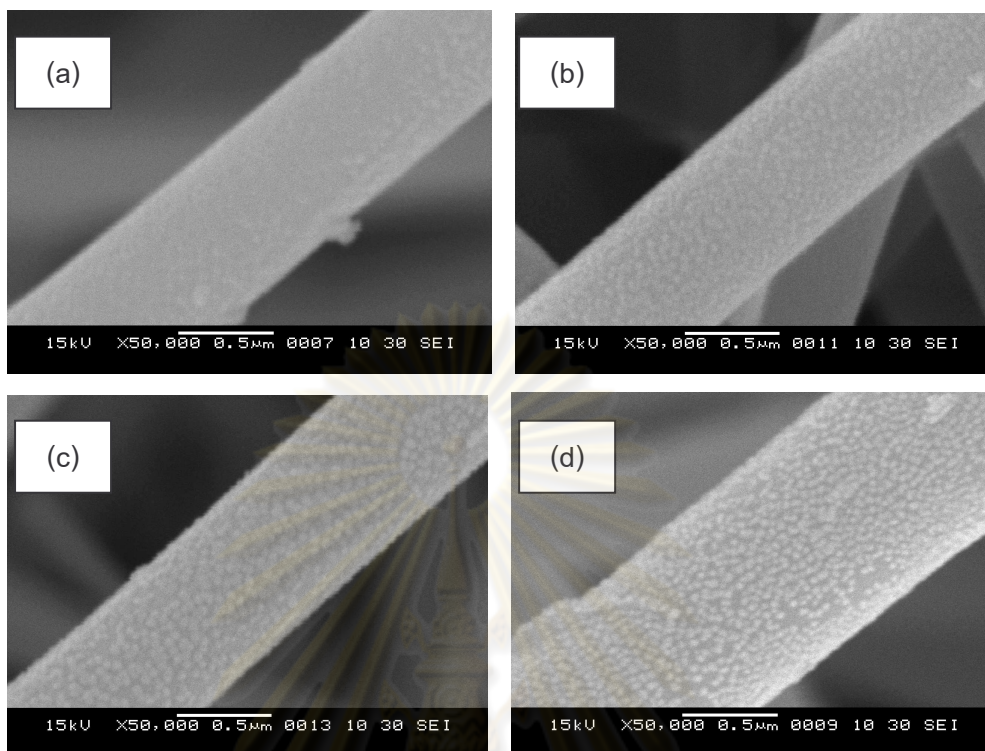
Figure 4.8 The SEM results of Co/SiO$_2$ fiber catalysts (a) 5 wt% (b) 10 wt% (c) 15 wt% (b) 20 wt%.

An energy dispersive spectroscopy (EDS) was used for calculation the element compositions of 5, 10, 15 and 20 wt% Co/SiO$_2$ fiber catalysts. Table 4.4 showed the cobalt content from the EDS analysis compared with the cobalt content required by the preparation. Results indicated that the preparation of 5 and 10 wt% Co/SiO$_2$ had actual content of cobalt deposited onto the silica fiber of 5.00 and 7.20 wt%, respectively. The higher cobalt content of 15 and 20 wt% Co/SiO$_2$ only contains the cobalt content of 8.68 and 8.04wt%, respectively. Because the submicron surface of fibers did not have the surface area enough to cobalt content at high level.

Table 4.4 Elemental analysis characterization of Co/SiO$_2$ fiber catalysts.

Cobalt/silica fibers	Wt% of cobalt
5 wt.%	5.00
10 wt.%	7.20
15 wt.%	8.68
20 wt.%	8.04
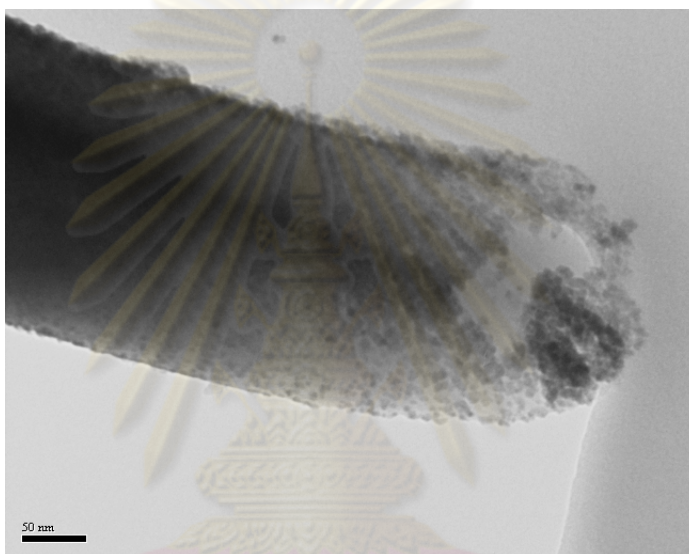
Figure 4.9 The TEM photograph of 10 wt% Co/SiO$_2$ fiber catalysts.

The transmission electron microscope (TEM) was used for determination of the surface morphology and dispersion of metal particles on the support. The TEM photograph of 10 wt% Co/SiO$_2$ fiber catalysts was shown in figure 4.9. Cobalt particles were spherical shapes. The morphology appearance of fiber catalyst could be clearly seen that cobalt particles were dispersed around silica fibers.
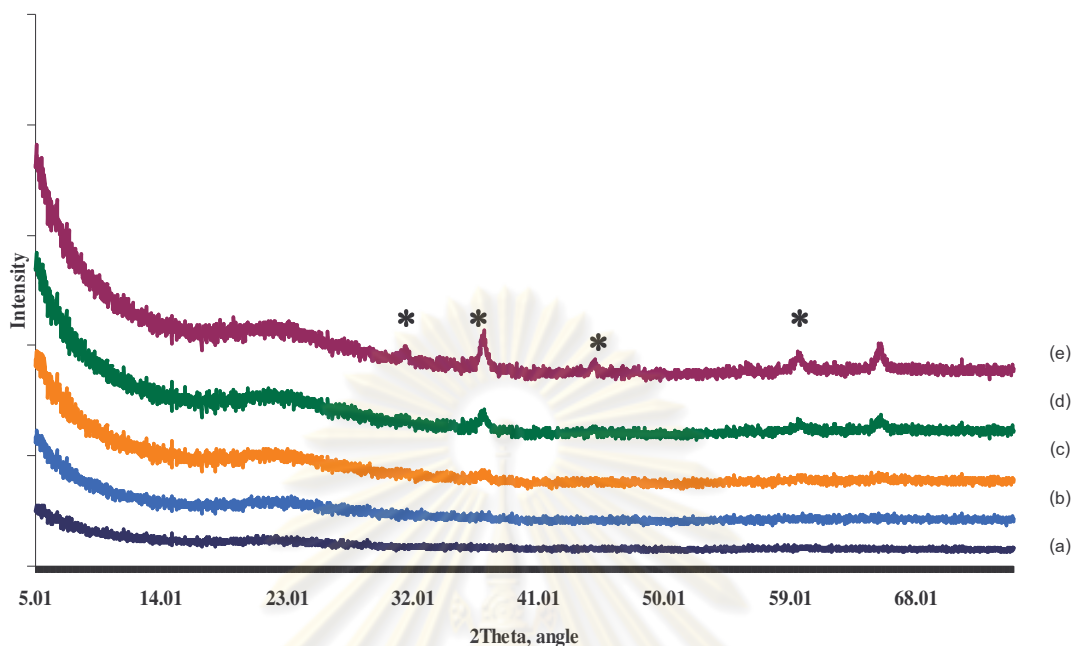
Figure 4.10 The XRD patterns of Co/SiO$_2$ catalysts calcined at 600°C for 2 h. (a) 10 wt% Co/SiO$_2$ porous, (b) 5 wt% Co/SiO$_2$ fiber, (c) 10 wt% Co/SiO$_2$ fiber, (d) 15 wt% Co/SiO$_2$ fiber, (e) 20 wt% Co/SiO$_2$ fiber.

X-ray diffraction was used for determination of the structure and crystallite size of catalyst. Results of the XRD patterns of the catalyst with different cobalt content calcined at 600°C for 2 h were shown in figure 4.10. The Co/SiO$_2$ catalyst after calcinations had the cobalt in form of the Co$_3$O$_4$. XRD peaks of Co$_3$O$_4$ were found at 31°, 37°, 45°, 59° and 65° [24]. The intensity of diffraction lines related to Co$_3$O$_4$ crystalline phase increased when cobalt content increased. The intensity diffraction lines of 20 wt% Co/SiO$_2$ was highest because the high cobalt content had the large Co$_3$O$_4$ crystalline and cobalt particles did not disperse well on silica fiber leading to the intensity diffraction lines increased.

4.1.5 The effect of reduction of Co/SiO$_2$ catalysts
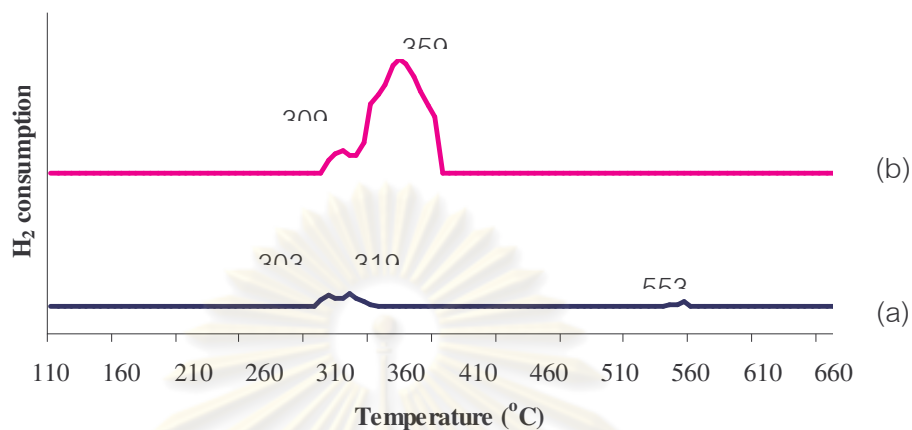
Figure 4.11 TPR profiles of Co/SiO$_2$ catalysts (a) 10wt% Co/SiO$_2$ porous catalyst (b) 10wt% Co/SiO$_2$ fiber catalyst.

Temperature-programmed reduction (TPR) was used for measurement of H$_2$ consumption. TPR profiles of 10 wt% Co/SiO$_2$ porous catalysts compared with 10 wt% Co/SiO$_2$ fiber catalyst was shown in figure 4.11(a) and (b), respectively. As shown in figure 4.11(a), three reduction peaks of TPR profile of 10 wt% Co/SiO$_2$ porous catalyst found reduction peaks at 303, 319 and 553°C. Reduction peaks at 303 and 319 ^{o}C were occurred by Co$_3$O$_4$ reduction (Co$_3$O$_4$→CoO→Co^o).Reduction peak at 553°C were occurred by cobalt (II) silicate [25]. Strong interaction between Co and silica support let to difficult reduction resulting in high temperature peak. As shown in figure 4.11(b), two reduction peaks of TPR profile of 10 wt% Co/SiO$_2$ fiber catalyst found reduction peaks at 309 and 359°C were occurred by Co$_3$O$_4$ reduction (Co$_3$O$_4$→CoO→Co^o). The degree of reduction was calculated by the equation 4.1 and summarized in table 4.5.

$$\text{Reduction degree (\%)} = 100 \times \frac{\text{mole of H}_2 \text{ consumption }_{measured}}{\text{mole of H}_2 \text{ consumption }_{calculated}} \quad (4.1)$$

For 10wt% Co/SiO$_2$ fiber catalysts the percentage of cobalt reduction was higher than 10wt% Co/SiO$_2$ porous catalysts. The results indicated that fiber catalysts could be reduced easily than porous catalysts.
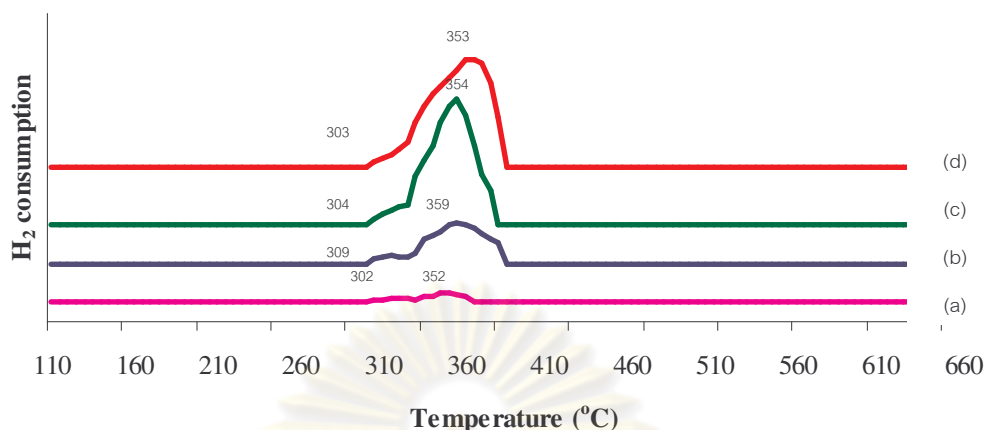
Figure 4.12 TPR profiles of Co/SiO_2 fiber catalysts with cobalt contents of (a) 5 wt% Co/SiO_2, (b) 10 wt% Co/SiO_2, (c) 15 wt% Co/SiO_2, (d) 20 wt% Co/SiO_2.

TPR profiles of Co/SiO_2 fiber catalyst with various cobalt contents (5-20wt %) was shown in figure 4.12(a), (b), (c) and (d), respectively. As shown in figure 4.12 two reduction peaks of TPR profile of Co/SiO_2 fiber catalyst were occurred by Co_3O_4 reduction ($Co_3O_4 \rightarrow CoO \rightarrow Co^o$). An increase of cobalt contents from 5 to 10wt%, let to an increase of the intensity of reduction peaks at high temperature because of the amount of Co_3O_4 increased. At 15 and 20 wt% cobalt, Reduction peaks at high temperature were very sharp. This result indicated that cobalt particles were clusters. The degree of reduction was calculated by the following equation 4.1 and summarized in table 4.5. An increase of cobalt content from 5 to 10 wt%, let to an increase of the percentage of cobalt reduction from 2.03% to 11.97% because of the lower cobalt content let to the small particle size reduction of cobalt and the interaction between the cobalt and silica support was stronger than the high cobalt content. An increase of cobalt content to 15 and 20 wt%, let to an increase of the percentage of cobalt d to 29.76% and 32.57%, respectively. The higher cobalt content let to the large particle size of cobalt cluster because the interaction between cobalt and silica support was weaker than the low cobalt content [26].

Table 4.5 The reduction degree of different catalysts calculated from TPR results.

Metal loading	Degree of Reduction (%)
5 wt% Co fiber	2.03
10 wt.% Co fiber	11.97
15 wt.% Co fiber	29.76
20 wt.% Co fiber	32.57
10 wt.% Co porous	0.89

4.2 CO hydrogenation

4.2.1 The effect of support: porous and fiber

Overall reaction $(2n+1) H_2 + n CO \rightarrow C_nH_{(2n+2)} + n H_2O$ (4.2)

Water gas shift reaction $H_2O + CO \rightarrow H_2 + CO_2$ (4.3)

Synthesis gas formation $CH_n + O_2 \rightarrow \frac{1}{2} H_2 + CO$ (4.4)
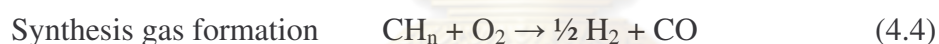
4.2.1.1 The effect of supporters on CO conversion

The effect of supports on CO conversion of 10 wt% Co/SiO_2 catalysts at 260^oC, 280^oC and 300^oC in CO hydrogenation was shown in figure 4.13(a) (b) and (c), respectively. As shown in Figure 4.13, CO conversion using silica fiber supporter at temperature 260^oC, 280^oC and 300^oC were 8.42%, 13.88% and 19.75%, respectively. CO conversion using silica fiber supporter was higher than using silica porous supporter. In contrast CO conversion using silica porous supporter at temperature 260^oC, 280^oC and 300^oC were 5.61%, 9.79% and 12.63%, respectively. An increase of pore size of the supporter, let to a decrease of CO conversion [27]. Result implied that the fiber supporter had no pores thus the CO conversion using silica fiber supporter was higher than using silica porous supporter.

Figure 4.13 Effect of supporters on CO conversion (%) of 10 wt%Co/SiO$_2$ catalysts at (a) 260°C (b) 280°C (c) 300°C and a feed flow rate 15 mL/min, catalyst loading 0.2 g and time 3 h(continue).

Figure 4.13 Effect of supporters on CO conversion (%) of 10 wt%Co/SiO$_2$ catalysts at (a) 260°C (b) 280°C (c) 300°C and a feed flow rate 15 mL/min, catalyst loading 0.2 g and time 3 h.

4.2.1.2 The effect of supporters on CH$_4$ selectivity

The effect of supporters on CH$_4$ selectivity of 10 wt% Co/SiO$_2$ catalysts at 260°C, 280°C and 300°C in CO hydrogenation was shown in figure 4.14(a) (b) and (c), respectively. As shown in figure 4.14, CH$_4$ selectivity using silica fiber supporter at temperature 260°C, 280°C and 300°C were 8.42%, 13.88%, respectively. CH$_4$ selectivity using silica fiber supporter was higher than using porous supporter. In contrast CH$_4$ selectivity using silica porous supporter at temperature 260°C, 280°C and 300°C were 75.58%, 82.68% and 86.46%, respectively. CH$_4$ selectivity and CO conversion trend were similar. The results indicated that the surface area of fiber supporter was lower than silica porous supporter. The fiber supporter did not have the surface area enough to supporter cobalt particles let to larger Co$_3$O$_4$ crystallites and the high reducibility of cobalt particles. Therefore, the interaction between the cobalt and silica support was weaker let to the easier and faster reaction.

Figure 4.14 Effect of supporters on CH$_4$ selectivity(%) of 10 wt% Co/SiO$_2$ catalysts at (a) 260°C (b) 280°C (c) 300°C and a feed flow rate 15 mL/min, catalyst loading 0.2 g and time 3 h(continue).

Figure 4.14 Effect of supporters on CH$_4$ selectivity(%) of 10 wt% Co/SiO$_2$ catalysts at (a) 260°C (b) 280°C (c) 300°C and a feed flow rate 15 mL/min, catalyst loading 0.2 g and time 3 h.

4.2.1.3 The effect of supporter on CO$_2$ selectivity

The effect of supporters on CO$_2$ selectivity of 10 wt% Co/SiO$_2$ catalysts at 260°C, 280°C and 300°C in CO hydrogenation was shown in figure 4.15(a) (b) and (c), respectively. As shown in figure 4.15, CO$_2$ selectivity using silica fiber supporter at temperature 260°C, 280°C and 300°C were 14.77%, 11.76% and 11.61%, respectively. CO$_2$ selectivity using silica fiber supporter was lower than using silica porous supporter. In contrast CO$_2$ selectivity using silica porous supporter at temperature 260°C, 280°C and 300°C were 24.42%, 17.32% and 13.54%, respectively. As equation 4.2, CO hydrogenation produced CH$_4$ and H$_2$O. H$_2$O was precursor of water gas shift reaction (equation 4.3). The silica porous supporter was more surface area to adsorb water molecules enough to react with CO by water gas shift step thus CO$_2$ selectivity using silica fiber supporter was lower than using silica porous supporter.
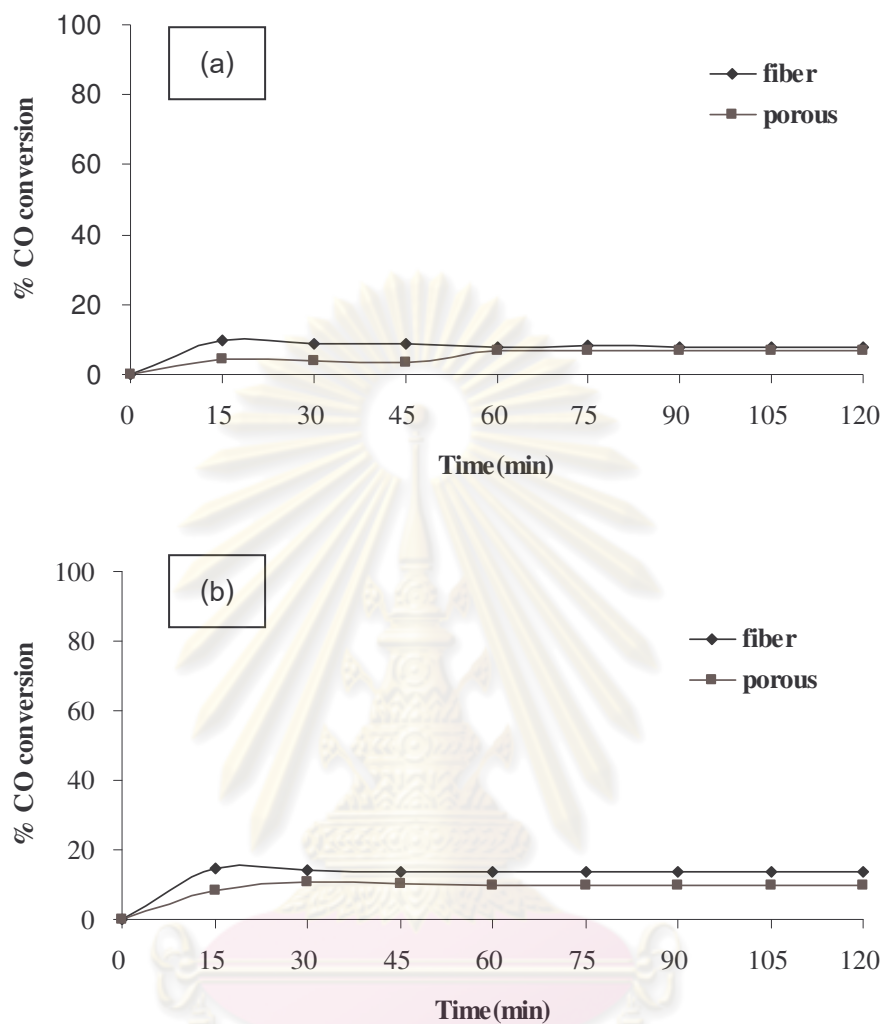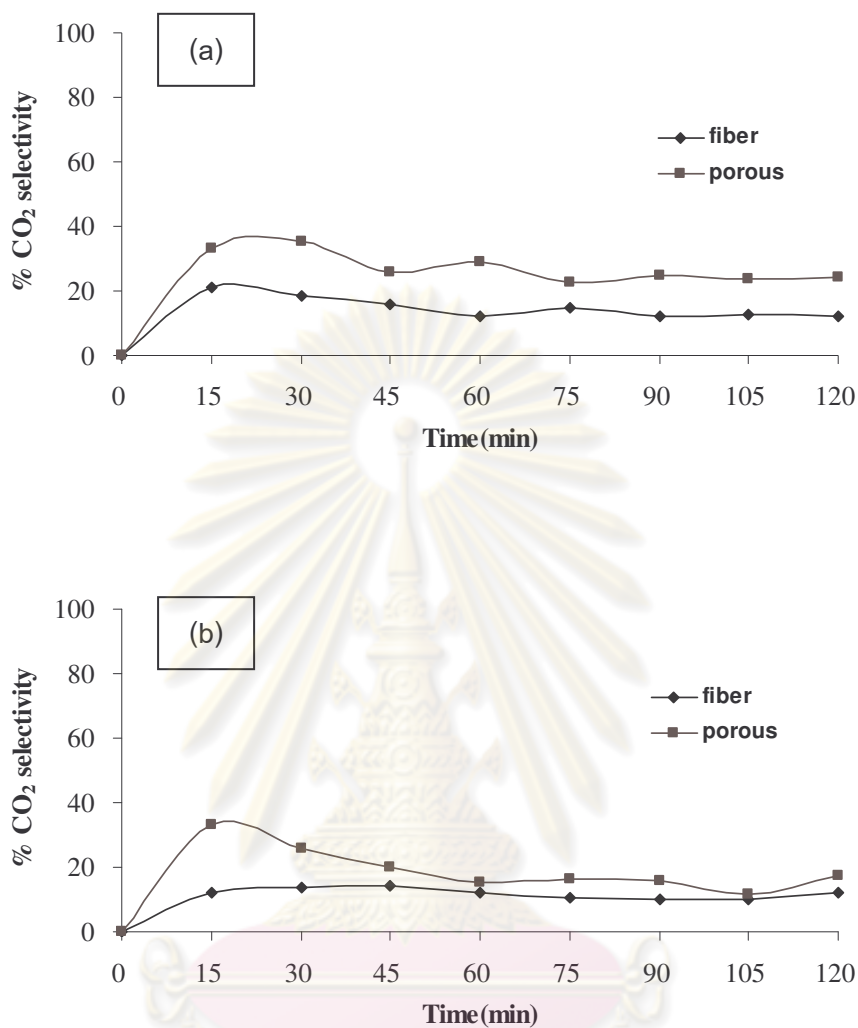
Figure 4.15 Effect of support on CO_2 selectivity (%) of 10wt%Co/SiO_2 catalysts at (a) 260°C (b) 280°C (c) 300°C and a feed flow rate 15 mL/min, catalyst loading 0.2 g and time 3 h (continue).
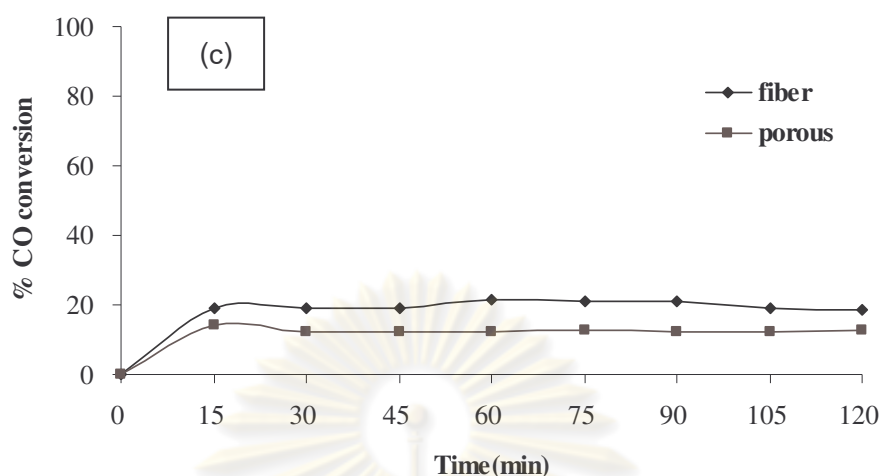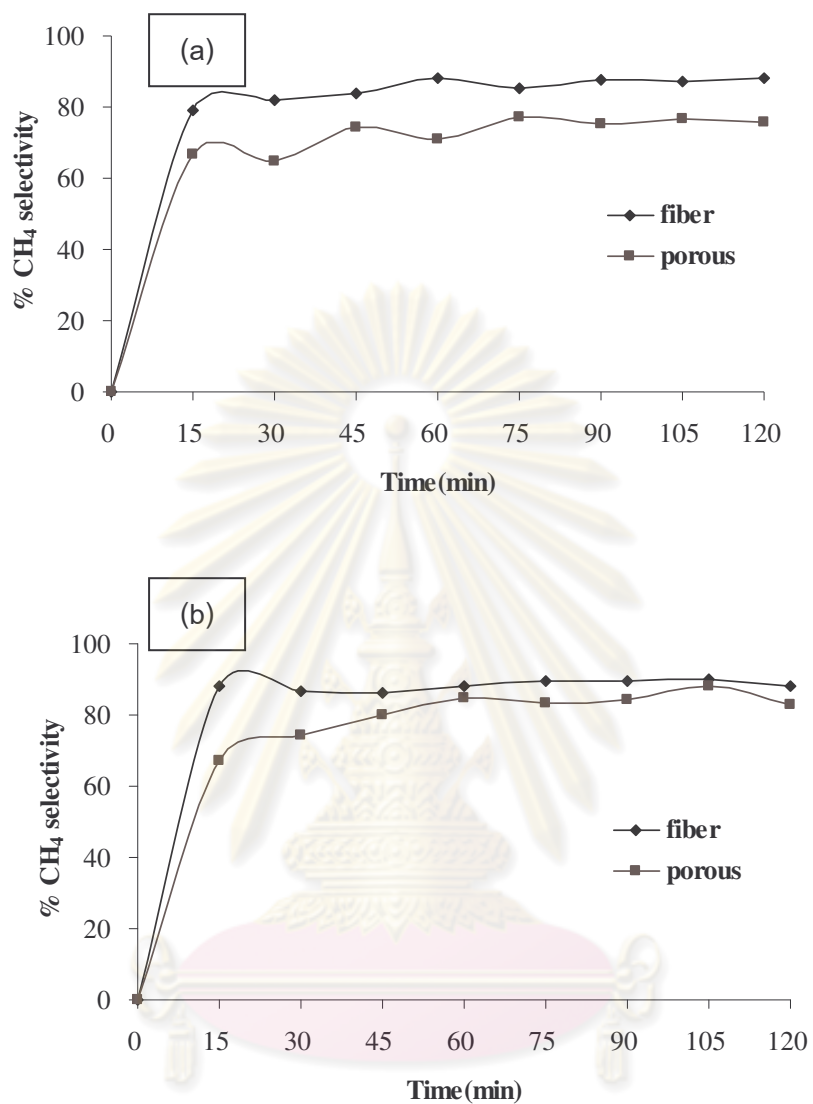
Figure 4.15 Effect of support on CO_2 selectivity (%) of 10wt%Co/SiO$_2$ catalysts at (a) 260°C (b) 280°C (c) 300°C and a feed flow rate 15 mL/min, catalyst loading 0.2 g and time 3 h.

Table 4.6 The effect of support: porous and fiber on the CO conversion, CH$_4$ selectivity and CO$_2$ selectivity.

Temperature (^{o}C)	% CO conversion		% CH$_4$ selectivity		% CO$_2$ selectivity	
	porous	fiber	porous	fiber	porous	fiber
260	5.61	8.42	75.58	85.23	24.42	14.77
280	9.79	13.88	82.68	88.24	17.32	11.76
300	12.63	19.75	86.46	88.39	13.54	11.61

4.2.2 The effect of reaction temperature.

The effect of reaction temperature on CO conversion, CH_4 selectivity and CO_2 selectivity of 10 wt% Co/SiO_2 fiber catalysts at 260^oC, 280^oC and 300^oC in CO hydrogenation was shown in figure 4.16, 4.17 and 4.18, respectively. As shown in figure 4.16 and 4.17, an increase of CO conversion and CH_4 selectivity, let to an increase of reaction temperature. At 300^oC reaction temperature, the highest CO conversion and CH_4 selectivity was 19.75% and 88.39%, respectively. CO hydrogenation was endothermic reaction [28] let to increment of reaction temperature resulting in conversion of CO and selective methane formation [26]. As shown in figure 4.18, a decrease of CO_2 selectivity, let to an increase of reaction temperature. As equation 4.2, CO hydrogenation produced CH_4 and H_2O. H_2O was precursor of water gas shift reaction (equation 4.3) and the carbon dioxide gas was produced. The water gas shift reaction was exothermic reaction let to increase the reaction temperature caused producing of H_2O and CO from equilibrium. Therefore, carbon dioxide was decreased [29].
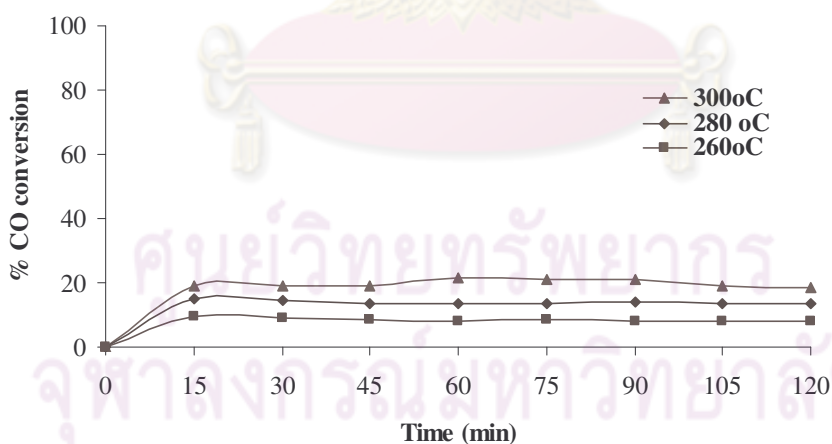
Figure 4.16 Comparison of the CO conversion (%) of 10 wt%Co/SiO_2 fiber catalysts at 260^oC, 280^oC and 300^oC and a feed flow rate 15 mL/min, catalyst loading 0.2 g and time 3h.
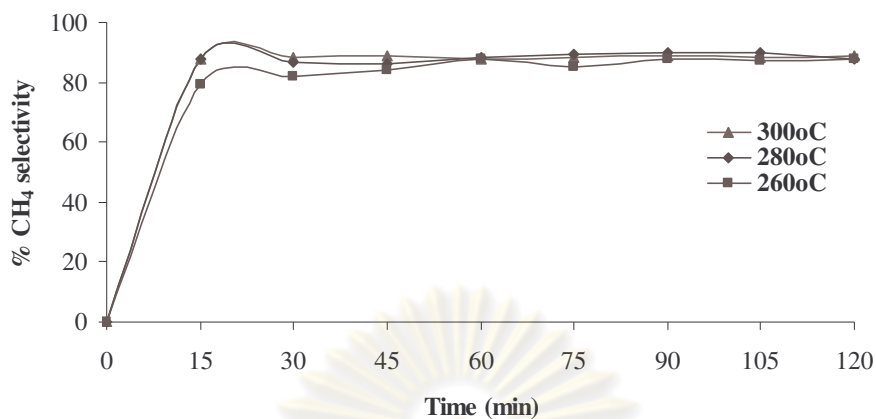
Figure 4.17 Comparison of the CH$_4$ selectivity (%) of 10 wt%Co/SiO$_2$ fiber catalysts at (a) 260°C (b) 280°C (c) 300°C and a feed flow rate 15 mL/min, catalyst loading 0.2 g and time 3h.
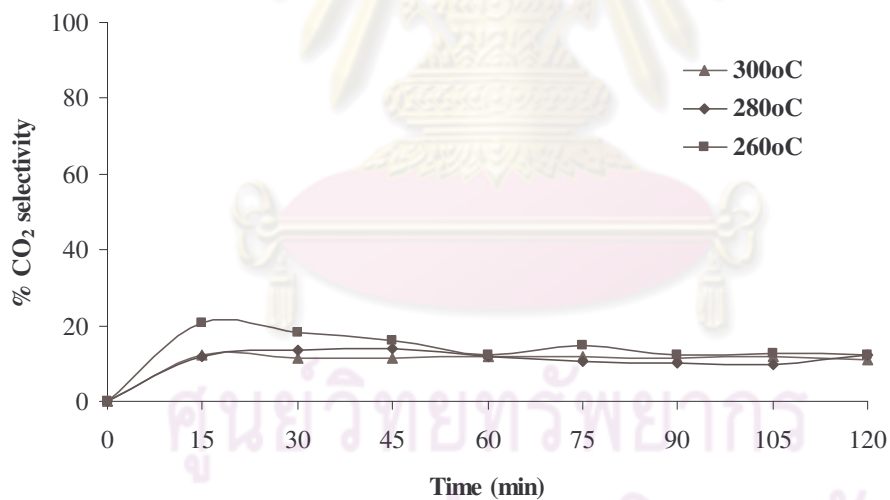
Figure 4.18 Comparison of the CO$_2$ selectivity (%) of 10 wt%Co/SiO$_2$ fiber catalysts at (a) 260°C (b) 280°C (c) 300°C and a feed flow rate 15 mL/min, catalyst loading 0.2 g and time 3h.

4.2.3 The effect of Co content.

The effect of cobalt content on CO conversion, CH_4 selectivity and CO_2 selectivity of 10 wt% Co/SiO_2 fiber catalysts at 260^oC, 280^oC and 300^oC in CO hydrogenation was shown in figure 4.19, 4.20 and 4.21, respectively. As shown in figure 4.19, an increase of cobalt content from 5 to 10 wt%, let to an increase of CO conversion from 10.43 to 19.75%. At the lower cobalt content of silica fiber, cobalt particles were small that the dispersion of cobalt particles was better than the high cobalt content. Thus the interaction between the cobalt and silica support was stronger let to the more difficult reaction than the high cobalt content. This indicated that the CO conversion was increased. Moreover, an increase of cobalt content to 15 and 20 wt%, let to a decrease of CO conversion to 11.19 and 9.56%. The large particles size of cobalt cluster let to the active cobalt of surface area was decreased. Therefore, CO conversion was decreased. As shown in figure 4.20 and 4.21, an increase of cobalt content, let to an increase of CH_4 selectivity and a decrease of CO_2 selectivity. An increase of cobalt content from 5 to 10wt%, let to an increase of CH_4 selectivity from 83.43 to 88.34% and a decrease of CO_2 selectivity from 16.57 to 11.66%. The value of CH_4 and CO_2 selectivity of 15 and 20wt% Co/SiO_2 fiber catalysts were quite similar. This indicated that the silica support had the average diameter size of 0.448 m can be loaded the cobalt content up to 10wt% because the EDS result was described the low surface area of fiber supporter for dispersion of cobalt particles.
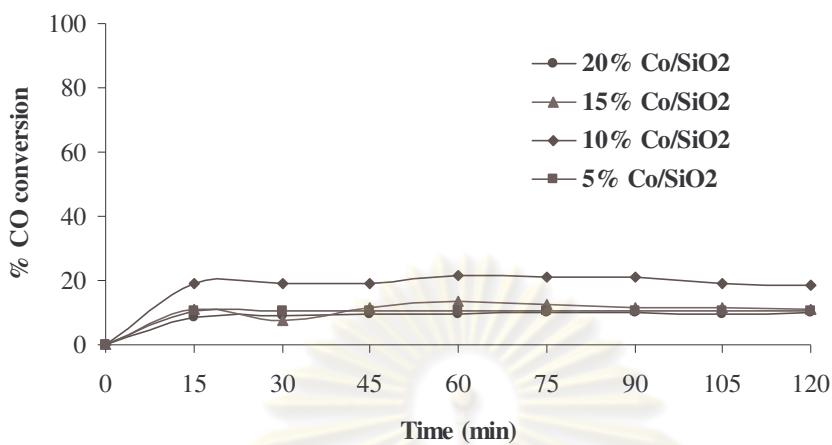
Figure 4.19 Comparison of Co content on the CO conversion (%) of Co/SiO$_2$ fiber catalysts varied Co content (5-20 wt %) at temperature 300°C, a feed flow rate 15 mL/min, catalyst loading 0.2 g and time 3 h.
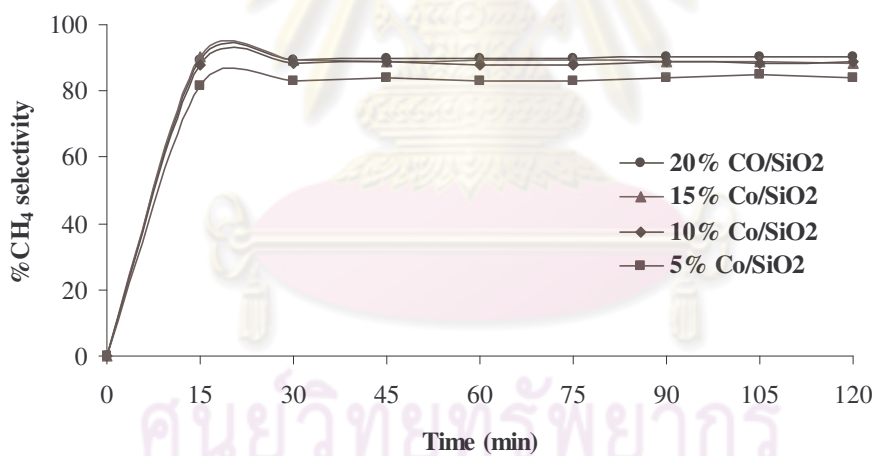
Figure 4.20 Comparison of Co content on the CH$_4$ selectivity (%) of Co/SiO$_2$ fiber catalysts varied Co content (5-20 wt %) at temperature 300°C, a feed flow rate 15 mL/min, catalyst loading 0.2 g and time 3 h.
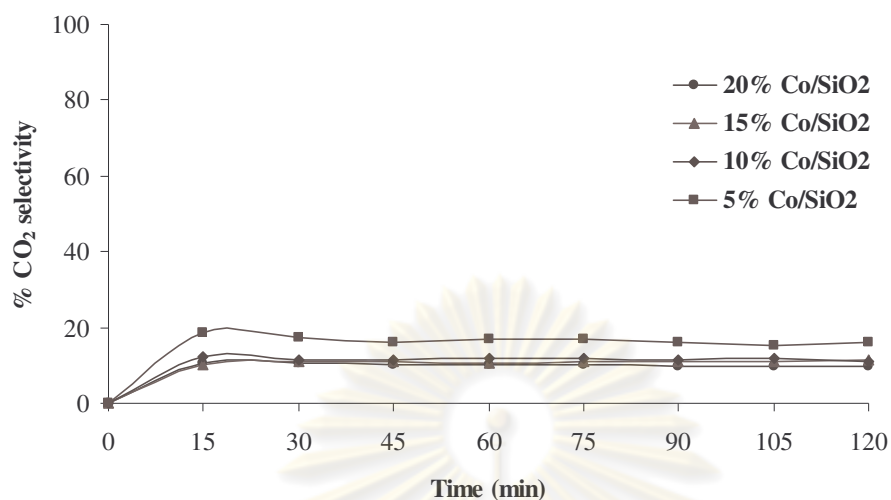
Figure 4.21 Comparison of Co content on the CO_2 selectivity (%) of Co/SiO_2 fiber catalysts varied Co content (5-20 wt %) at temperature $300^{o}C$, a feed flow rate 15 mL/min, catalyst loading 0.2 g and time 3 h.

Table 4.7 The effect of Co content (5-20 wt %) on the CO conversion, CH_4 selectivity and CO_2 selectivity.

%Co	%CO conversion	%Selectivity	
		CH_4	CO_2
5	10.43	83.43	16.57
10	19.75	88.34	11.66
15	11.19	89.15	10.85
20	9.56	89.94	10.06

4.3 An advantage and disadvantage of fiber catalyst

Advantage

1. A problem solving of the condensation of products to block pores catalyst was deactivated and pressure drop.
2. The fiber catalyst could produce more methane in CO hydrogenation.

Disadvantage

1. Difficult fiber preparation by electrospinning technique.

4.4 Comparison between this thesis with other thesis

1. This thesis used fiber catalyst for CO hydrogenation but other thesis used porous catalyst for CO hydrogenation.
2. The main product of CO hydrogenation at atmospheric pressure was CH_4 in this thesis but CO hydrogenation in other thesis did not at atmospheric pressure.

ศูนย์วิทยทรัพยากร
จุฬาลงกรณ์มหาวิทยาลัย

CHAPTER V

CONCLUSION AND RECOMMENDATION

5.1 Conclusion

The Co/SiO_2 fiber catalyst was success with prepared by electrospinning with impregnation. The diameters of electrospun fibers after calcinations were decreased. The average diameter of fibers depended on needle size, the percentage of PVP content, the tip to collector distance and the voltage. The higher the needle size and PVP content, The smaller the average diameter of electrospun fiber was obtained. The optimum condition of electrospinning was needle size at 0.4 mm, PVP content at 70wt%, voltage at 20 kV and the tip to collector distance at 15 cm. The average diameter of the electrospun fibers were 0.448 μm. The surface area result (BET) showed the porous silica was $237.36m^2/g$ and the silica fiber was $2.76m^2/g$. The surface area morphology of Co/SiO_2 fiber catalyst was rough because the cobalt particles were dispersed over the silica fibers. The clusters of cobalt particles were observed at higher cobalt content. Because the submicron surface of fibers did not have the surface area enough to cobalt content at high level. The crystallized phases as studied by XRD after calcinations to the Co_3O_4 were observed. The element composition was confirmed by EDS. Three reduction peaks of TPR profile porous catalyst found reduction peaks at 303, 319 and 553^oC. Reduction peaks at 303 and 319^oC were occurred by Co_3O_4 reduction $(Co_3O_4 \rightarrow CoO \rightarrow Co^o)$.Reduction peak at 553^oC were occurred by cobalt (II) silicate. Two reduction peaks of TPR profile of fiber catalyst found reduction peaks at 309 and 359^oC were occurred by Co_3O_4 reduction $(Co_3O_4 \rightarrow CoO \rightarrow Co^o)$.The degree of reduction of the fiber catalyst was higher than the porous catalyst. An increase of the degree of reduction of fiber catalysts, let to an increase of cobalt content. The higher cobalt content let to the large particle size of cobalt cluster because the interaction between cobalt and silica support was weaker than the low cobalt content. In CO hydrogenation, CO conversion and CH_4 selectivity of the fiber catalyst was higher than the porous catalyst. In contrast CO_2 selectivity of

the fiber catalyst was lower than the porous catalyst. CO hydrogenation produced CH_4 and H_2O. H_2O was precursor of water gas shift reaction. The porous supporter was more surface area to adsorb water molecules enough to react with CO by water gas shift step thus CO_2 selectivity of the porous catalyst was higher than the fiber catalyst. CO conversion of 10wt% Co/SiO_2 fiber catalyst was highest. The value of CH_4 and CO_2 selectivity of 15 and 20wt% Co/SiO_2 fiber catalysts were quite similar. This indicated that the silica support had the average diameter size of 0.448 μm can be loaded the cobalt content up to 10wt% because the EDS result was described the low surface area of fiber supporter for dispersion of cobalt particles. 10 wt% Co/SiO_2 fiber catalyst was the best catalyst for CO hydrogenation in this study.

5.2 Recommendation

For the future research work, the fiber in small diameter was produced using electrospinning process developed by decreasing the needle and increasing PVP content. For comparison with fiber catalysts were prepared by impregnation method with cobalt acetate with cobalt nitrate in CO hydrogenation.

REFERENCES

[1]   Yi, Z., Yong, L., Guohui Y., Shouli, S., Noritatsu, T. Effects of impregnation solvent on Co/SiO$_2$ catalyst for Fischer-Tropsch synthesis: A highly active and stable catalyst with bimodal sized cobalt particles. Applied Catalysis A: General. 321(2007): 79–85.

[2]   Sukamon, H., Yi, Z., Satosh, N., Tharapong, V., Noritatsu, T. TiO$_2$ promoted Co/SiO$_2$ catalysts for Fischer–Tropsch synthesis. Fuel Processing Technology. 9(2008): 455-459.

[3]   Choi, S. Titania-Doped silica fibers prepared by electrospining and sol-gel process. Journal of Sol-gel Science and Technology. 30: (2004) 215-221

[4]   Ken Mauritz. Sol-Gel Chemistry. [online]. Available from: http://www.pscr.us m.edu/mauritz/solgel.html. [2004, Febuary 25]

[5]   Alain, C., P. Introduction to sol-gel processing. Boston: Kluwer Academic Publishers,. 1998.

[6]   C., Jeffrey, B., George, W., S. Sol-gel science the physics and chemistry of sol-gel processing. Boston: Academic Press, Inc,. 1990.

[7]   Lisa, C., K. Sol-gel technology for thin films, fibers, performs, electronics and Specialty shapes. New Jersey: Noyes Publications,.1998.

[8]   Seeram, R., Kazutoshi, F.,Wee-Eong, T.,Teik-Cheng, L., Zuwei, M. An Introduction to Electrospinning and Nanofibers. Singapore: World Scientific Publishing Co. Pte. Lte., 2005.

[9]   Devid, F., C. Electrospinning [online]. Available from: http://www.che.vt.edu/ wilkes/electrospinning/electrspinning.html. [2009, October 4]

[10]   Wikipedia. Fischer-Tropsch process [online]. Available from: http://en.wikipedia.org/wiki/Fischer%E2%80%93Tropsch process. [2010, March 16]

[11]   U.S. Department of Energy. The Early Days of Coal Research [online]. Available from: http://www.fe.doe.gov/aboutus/history/syntheticfuels.html [2010, March 18]

[12]   Andre, S., Mark, D. Fischer-Tropsch Technology. United Kingdom: Elesevier,. 2004.

[13]   Barbara, E., Suzanne, L., Patrick, C., Alain, K. Preparation and characterization of Fischer–Tropsch active Co/SiO$_2$ catalysts. Applied Catalysis A: General. 186(1999): 145–168.

[14]   Dala, A., K., Davis, B., H. Fischer–Tropsch synthesis: A review of water   effects on the performances of unsupported and supported Co catalysts. Applied Catalysis A: General. 348(2008): 1–15.

[15]   Koski, A., Yim, K., Shivkumar, S. Effect of molecular weight on fibrous PVA produced by electrospinning. Journal of Material. 58(2004): 493-497.

[16]   Changlu, S., Hak,Y., K., Jian, G., Bin, D., Douk, R., L., Soo, J., P. Fiber mats of poly(vinyl alcohol)/silica composite via electrospinning. Journal of material. 57(2003): 1579-1584.

[17]   Hongyu, G., Changlu, S., Shangbin, W., Bin, C., Jian, G., Xinghua,Y. A novel method for preparing Co$_3$O$_4$ nanofibers by using electrospun PVA cobalt acetate composite fibers as precursor. Materials Chemistry and Physics. 82(2003): 1002–1006.

[18]   Xinghua, Y., Changlu, S., Hongyu, G., Xiliang, L., Jian, G. Preparation and characterization of ZnO nanofibers by using electrospun PVA/zinc acetate composite fiber as precursor. Inorganic Chemistry Communications. 7(2004): 176–178.

[19]   Shi, L., Li, D., Hou, B., Sun, Y. Organic Modification of SiO_2 and Its Influence on the Properties of Co-Based Catalysts for Fischer–Tropsch Synthesis. Chiness Journal of Catalysis. 28(2007): 999–1002.

[20]   Wan, H., J., Wu, B., S., Tao, Z., C., Li, T., Z., Ana, X., Xiang, H., W., Li, Y., W. Study of an iron-based Fischer-Tropsh synthesis catalyst incorporated with SiO_2. Journal of Molecular Catalysis A: Chemical. 260(2006): 255-263.

[21]   Song, D., Li, J. Effect of catalyst pore size on the catalytic performance of silica supported cobalt Fischer–Tropsch catalysts. Journal of Molecular Catalysis A: Chemical. 247(2006): 206-212.

[22]   Bae, J., Kim, S., M., Kang, S., H., Chary, K., V., R., Lee, Y., j., Kim, H., J., Jun, K., W. Effect of support and cobalt precursors on the $Co/AlPO_4$ catalyst in Fischer-Tropsch synthesis. Journal of Molecular Catalysis A: Chemical. 311(2009): 7-16.

[23]   Peng, K., Zhou, L., Hu, A., Tang, Y., Li, D. Synthesis and magnetic properties of $Ni-SiO_2$ nanocomposites. Material Chemistry and Physics. 111(2008): 34-37.

[24]   Khodakov, A., Y., Lynch, J., Bazin, D., Rebours, B., Zanier, N., Moisson, B., Chaumette, P. Reducibility of Cobalt Species in Silica-Supported Fischer–Tropsch Catalysts. Journal of Catalysis. 168 (1997), 16–25.

[25]   Agustin, M., Carlos, L., Francisco, M., Isabel, D. Fischer–Tropsch synthesis of hydrocarbons over mesoporous Co/SBA-15 catalysts: the influence of metal loading, cobalt precursor, and promoters. Journal of Catalysis. 220 (2003): 486–499.

[26]   Giovanni, B., Claudia, C., Maria, T., Serena, E., Antonio, A., Pasquale, P. TPR/TPO characterization of cobalt–silicon mixed oxide nanocomposites prepared by sol–gel. Thermochimica Acta. 471(2008): 51–54.

[27]   Shouli, S., Noritatsu, T., Kaoru, F. The reaction performances and characterization of Fischer–Tropsch synthesis Co/SiO_2 catalysts prepared from mixed cobalt salts. Applied Catalysis A: General. 202(2000): 121–131.

[28]   James, G., S. Synthetic fuels handbook: properties, process, and performance. New York: The McGraw-Hill companies, Incorporation., 2008.

[29]   Chemical equilibrium [online]. Available from: http://elearning.spu.ac.th/content/chm100/chm/100_ch11.html. [2010, January 29]

APPENDIXES

Appendix A

Calculation for preparation of 10wt% Co/SiO$_2$ fiber catalyst

10wt% Co/SiO$_2$ fiber catalyst was prepared by electrospinning (sol-gel), polymer dilution technique and impregnation method.

1st step: electrospinning (sol-gel)

	MW(g/mol)	Density(g/cm^3)
Silica (SiO$_2$)	60.09	2.20
EtOH	46.07	0.789
H$_2$O	18.00	1.00
HCl	36.46	1.18
TEOS(purity 98%)	208.33	0.933

TEOS 1 mol = silica 1 mol

Assume of silica 7.5 g

Therefore, weight of TEOS = (208.33 x 7.5)/60.09 = 26.00 g

$\qquad\qquad\qquad$ = 26.00/208.33 mol

$\qquad\qquad\qquad$ = 0.1248 mol

For sol-gel The mol ratio of TEOS:EtOH:H$_2$O:HCl = 1:2:2:0.1

At TEOS = 0.1248 mol

Thus TEOS:EtOH:H$_2$O:HCl = 0.1248:0.2494:0.2494:1.2x10^{-3}

From   mol = volume x density

Therefore, EtOH = 0.2494 mol $\qquad$ = (0.2494 x 46.07)/0.789 mL

$\qquad\qquad\qquad\qquad\qquad\qquad$ = $\underline{14.56\ mL}$

$\quad$ H$_2$O = 0.2494 mol $\qquad$ = (0.2494 x 18)/1 mL

$\qquad\qquad\qquad\qquad\qquad\qquad$ = $\underline{14.56\ mL}$

$\qquad\qquad$ HCl = 1.2x10^{-3} mol $\qquad$ = (1.2x10^{-3} x 36.46)/1.18 mL

$$= \underline{0.04 \text{ mL}}$$

From   mol = (10 x Density x purity x volume)/(1000 x MW)

Therefore, TEOS = 0.1248 mol   = (10 x 0.933 x 0.98 x Volume)/(1000 x 208.33)

Volume $= \underline{28.53 \text{ mL}}$

2nd step: polymer dilution

5wt% PVP/EtOH = EtOH 100 g was have PVP 5 g

Assum of EtOH = 5 g

Therefore, weight of PVP = 5 x 5 /100 g

$= \underline{0.25 \text{ g}}$

3rd step: impregnation

TEOS(purity 98%) (MW = 208.33 g/mol, Molecular formula = $SiC_8H_{20}O_4$ and density = 0.933 g/cm^3)

The mol ratio of TEOS:EtOH:H_2O:HCl = 1:2:2:0.1

From   mol = volume x density

At 1st step TEOS 0.1248 mol = 28.53 mL

Using TEOS 1 mol   = (28.53 x 1)/0.1248 mL

= 228.61 mL

= 228.61 x 0.933 g

$= \underline{213.29 \text{ g}}$

Calculate volume of SiO$_2$ in TEOS

At 1st step SiO$_2$ (MW = 60.09 g/mol)

TEOS 1 mol   = silica 1 mol

TEOS 208.33 g = SiO$_2$ 60.09 g

Therefore,   TEOS 213.29g = SiO$_2$ (60.09 x 213.29)/208.33 g

= SiO$_2$ $\underline{61.52 \text{ g}}$

Calculate volume of SiO$_2$ in silica fiber and volume of cobalt (II) acetate Co (CH$_3$COO)$_2$.4H$_2$O for 10wt% Co/SiO$_2$

Assume of fiber = 0.05 g

	Fiber 1 mol	= TEOS 1 mol
From above	TEOS 213.29 g	= SiO$_2$ 61.52 g
Therefore,	Fiber 213.29 g	= SiO$_2$ 61.52 g
	Fiber 0.05 g	= SiO$_2$ (61.52 x 0.05)/213.29 g
		= SiO$_2$ 0.014 g

Co (MW = 58.93 g/mol) and Co (CH$_3$COO)$_2$.4H$_2$O (MW = 249.09 g/mol)

Assume 10wt% Co/SiO$_2$: SiO$_2$ 90 g + Co 10 g

Therefore,	SiO$_2$ 90 g	= Co 10 g
	SiO$_2$ 0.014 g	= Co (10 x 0.014)/90 g
		= Co 0.0016 g
Co 1 mol	= Co(CH$_3$COO)$_2$.4H$_2$O 1 mol	
Therefore,	Co 58.93 g	= Co(CH$_3$COO)$_2$.4H$_2$O 249.09 g
From above	Co 0.0016 g	= Co(CH$_3$COO)$_2$.4H$_2$O (249.09 x 0.0016)/58.93 g
		= Co(CH$_3$COO)$_2$.4H$_2$O 0.045 g

Calculate volume of catalyst for wet impregnation

Co (MW = 58.93 g/mol) and Co(CH$_3$COO)$_2$.4H$_2$O (MW = 249.09 g/mol)

Pore volume of silica gel = 1.12 mL/g

Assume silica gel = 5 g

10wt% Co/SiO$_2$: silica gel 90 g + Co 10 g

Therefore,	silica gel 90 g	= Co 10 g
	silica gel 5 g	= Co (10 x 5)/90 g
		= Co 0.556 g

Co 1 mol	= Co(CH$_3$COO)$_2$.4H$_2$O 1 mol	
Therefore,	Co 58.93 g	= Co(CH$_3$COO)$_2$.4H$_2$O 249.09 g
From above	Co 0.556 g	= Co(CH$_3$COO)$_2$.4H$_2$O (249.09 x 0.556)/58.93 g

$$= Co(CH_3COO)_2.4H_2O \quad \underline{2.35 \text{ g}}$$

Pore volume of silica gel = 1.12 mL/g

Therefore, silica gel 1 g in volume of solution 1.12 mL

From above Assume silica gel = 5 g

Thus,   silica gel 5 g in volume of solution (1.12 x 5)/1 mL

          volume of solution = 5.6 mL

Calculate of   the surface area of SiO$_2$ fiber

Silica fiber produced by needle size of 0.4 mm, TCD of 15 cm, voltage of 15 kV and PVP content = 70wt%.

Average diameter (from SEM image) = 0.448 μm. Therefore radius = 0.448/2 μm.

= 0.224 μm.

Density of SiO$_2$ = 2.1 g/cm^3

Character of surface area of fiber was cylinder.

Surface area of cylinder = 2πrh (r = radius and h = high)

Volume of cylinder = πr^{2}h (r = radius and h = high)

Thus, Surface area = area/g

From   mol = volume x density

Surface area/(volume x density)   m^2/g

$$= 2 \text{ } rh/ \text{ } r^2h \times density) \quad m^2/g$$
$$= 2/(r \times density) \quad\quad m^2/g$$
$$= 2/(0.224 \times 2.1) \quad\quad m^2/g$$
$$= \underline{4.25 \text{ } m^2/g}$$

Calculate reduction degree (%)

Catalyst: 10wt% Co/SiO$_2$ fiber catalyst

Flow rate of H$_2$ = 30 mL/min from 5% H$_2$ in N$_2$

Therefore,   Flow rate of H$_2$ = 0.05 x 30 = 1.5 mL H$_2$ /min

At STP   1 mol = 22.4 L = 22400 mL

Therefore,   22400 mL   = 1 mol H_2 /min

                1.5 mL   = (1 x 1.5)/ 22400 mol H_2 /min

                                 = 0.000066964 mol H_2 /min

Assum area of H_2 before reduced   = 104470 area/min

Mole of H_2 = 0.000111607 mol

Area of H_2 after reduced   = 27983.85 mol H_2

                                 = (27983.85 x 0.000111607)/ 104470

                                 = 0.000029896 mol H_2 (was usable to real)

Mole of Co   = 58.93

Mole of CoO   = 74.93

Mole of SiO_2 = 60.09

CoO/Co   = 1.27151

Co/ SiO_2 = 10(100-10)

                              = 0.1111

CoO/ SiO_2 = 1.27151 x 0.1111

                              = 0.141279

10wt% Co/SiO_2 fiber catalyst = 0.1 g

Thus,   CoO + SiO_2 = 0.1 g

               (CoO/ SiO_2) + (SiO_2/ SiO_2)   = 0.1/ SiO_2

Therefore,   0.141279 + 1 = 0.1// SiO_2

                    SiO_2 = 0.087621

Then CoO + SiO_2 = 0.1 g   thus   CoO = 0.1 – 0.087621

                                    = 0.012379 g

                                    = 0.012379/ 74.93 mol

                                    = 0.000165 mol H_2 (was usable to theory)

% reduction = mol H_2 (real)/ mol H_2 (theory) x 100

                = 0.000029896 / 0.000165 x 100

= 18.12 %

Calculatation of CO conversion, CH₄ selectivity and CO₂ selectivity of Fischer-Tropsch reaction.

From $\quad PV = nRT$

P = pressure (atm), V = volume (L), n = mole (mol), R = constant and T = temperature (K)

Assum Condition

Catalyst	10wt% Co/SiO₂ fiber catalyst
Weight of catalyst	0.2 g
Feed flow rate	15 mL/min
Temperature	25°C = 298 K
Temperature reaction	260 °C
Pressure	1 atm
R (constant)	0.0820513 atm L /mol K
Volume input (V_{in})	15 mL/min
Mole input (n_{in})	= (1 x 0.015)/(0.0820513 x 298)
	= 0.000613 mol/min

Component (n_{in})	wt%	mol
H_2	65	= (65 x 0.000613)/100 = 0.000398
CO	32	= (32 x 0.000613)/100 = 0.000196
Ar	3	= (3 x 0.000613)/100 =1.84 x 10⁻⁵

Volume out put (V_{out})	= 15 mL/min
Mole out put (n_{out})	= (1 x 0.015)/(0.0820513 x 298)
	= 0.000613 mol/min

Area of synthesis gas (before reaction)

No.	Area			
	H_2	Ar	CO	CO/Ar
1	9394.8	25250.3	157429.7	6.23
2	9331.7	24261.7	157711.8	6.50
			Average	6.37

After reaction at 60 min

Temperature	Area					
	H_2	Ar	CO	CH_4	CO_2	CO/Ar
60^oC	3947.1	27382.2	159678.6	947.2	251.3	5.83

Therefore, % CO conversion = (6.37 – 5.83)/6.37 x 100 %

= 8.48 %

Area of standard gas

No.	CH_4 20 wt%	CO 20 wt%	CO_2 100wt%
1	74434.3	132700.5	535815.9
2	75807	132759.6	541264.5
Average	75120.65	132730.05	538540.2

From $PV = nRT$

P = pressure (atm), V = volume (L), n = mole (mol), R = constant and T = temperature (K)

$n = PV/RT$

Therefore, (n_{Out})

Mole of CO $= (159678.6 \times 20)/132730.05 = 24.06 \%$

$= ((24.06/100) \times 0.015)/(0.0820513 \times 298)$ mol

$= 0.0001476$ mol

Mole of CH_4 $= (947.2 \times 20)/75120.65 = 0.252 \%$

$= ((0.252/100) \times 0.015)/(0.0820513 \times 298)$ mol

$= 0.0000015$ mol

Mole of CO_2 $= (251.3 \times 100)/ 538540.2 = 0.047 \%$

$= ((0.047/100) \times 0.015)/(0.0820513 \times 298)$ mol

$= 0.0000003$ mol

% CH_4 selectivity $= (0.0000015/ (0.0000015 + 0.0000003)) \times 100$

$= 83.33 \%$

%CO_2 selectivity $= (0.0000003 / (0.0000003 + 0.0000015)) \times 100$
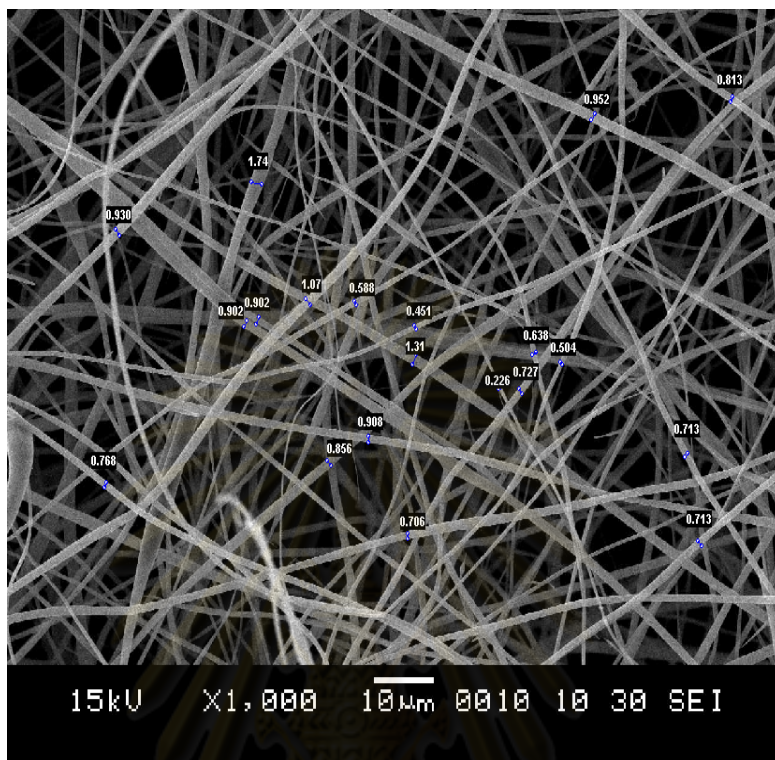
$= 16.67 \%$

Appendix B

Figure B-1 Determination of fiber diameter by SemAfore program

Figure B-2 Gas chromatography.

Table B-1 Determination of CO conversion and gas product selectivity.

Data from the use of catalyst: 10wt% Co/ SiO$_2$ porous catalyst

Temperature of reaction = 260°C

Feed flow rate 15 mL/min, Weight of catalyst = 0.2 g

Standard gas composition: 20wt% CO, 20wt% CH$_4$ 100wt% CO$_2$ balance in He

Area	std	15	30	45	60	75	90	105	120
H$_2$		3961.3	3982.4	4002.8	4009.2	3944.6	3999.6	3983.6	3911.4
Ar		26346.7	26212.2	26093	26999.9	26976.8	26995.7	26914.8	26855.9
CO	132730.1	160313.5	160686.8	160734.2	160610.5	160411.9	160414.9	159711.7	159391.4
CH$_4$	75120.65	226.4	195.9	222.7	239	247.9	255.7	242.6	245
CO$_2$	538540.2	162.2	151.9	110.5	138.7	104.5	119.7	106.5	113.5

Min		15	30	45	60	75	90	105	120
Mole	CO	0.0001483	0.0001483	0.0001476	0.0001477	0.0001476	0.0001484	0.0001483	0.0001482
	CH$_4$	0.0000004	0.0000003	0.0000004	0.0000004	0.0000004	0.0000004	0.0000004	0.0000004
	CO$_2$	0.0000002	0.0000002	0.0000001	0.0000002	0.0000001	0.0000001	0.0000001	0.0000001
% CO conversion		4.44	3.73	3.26	6.58	6.62	6.68	6.81	6.79
% Selectivity	CH$_4$	66.68	64.90	74.29	71.19	77.28	75.39	76.56	75.58
	CO$_2$	33.32	35.10	25.71	28.81	22.72	24.61	23.44	24.42

Table B-2 Determination of CO conversion and gas product selectivity.

Data from the use of catalyst: 10wt% Co/ SiO_2 porous catalyst

Temperature of reaction = $280^{o}C$

Feed flow rate 15 mL/min, Weight of catalyst = 0.2 g

Standard gas composition: 20wt% CO, 20wt% CH_4 100wt% CO_2 balance in He

Area	std	15	30	45	60	75	90	105	120
H_2		3932.4	3981.1	3958	3935.5	4001.1	3957	3941.3	3975.2
Ar		26074.7	26839.3	26660.3	26590.4	26549.7	26444.6	26470.4	26368.3
CO	147422.9	160473.2	160150.2	159949.9	160401.3	160293.2	160257.1	160018.5	159730.9
CH_4	82670.8	317.2	381.4	464.2	481.6	538.9	507.1	549.3	562.2
CO_2	551982.35	208.4	178.2	156.6	115.4	142.8	126.0	97.1	157.3

Min		15	30	45	60	75	90	105	120
	CO	0.0001336	0.0001333	0.0001331	0.0001335	0.0001334	0.0001334	0.0001332	0.0001329
Mole	CH_4	0.0000005	0.0000006	0.0000007	0.0000007	0.0000008	0.0000008	0.0000008	0.0000008
	CO_2	0.0000002	0.0000002	0.0000002	0.0000001	0.0000002	0.0000001	0.0000001	0.0000002
% CO conversion		8.14	10.94	10.46	9.97	9.89	9.55	9.77	9.59
% Selectivity	CH_4	67.02	74.08	79.83	84.79	83.44	84.31	88.31	82.68
	CO_2	32.98	25.92	20.17	15.21	16.56	15.69	11.69	17.32

Table B-3 Determination of CO conversion and gas product selectivity.

Data from the use of catalyst: 10wt% Co/ SiO$_2$ porous catalyst

Temperature of reaction = 300°C

Feed flow rate 15 mL/min, Weight of catalyst = 0.2 g

Standard gas composition: 20wt% CO, 20wt% CH$_4$ 100wt% CO$_2$ balance in He

Area	std	15	30	45	60	75	90	105	120
H$_2$		4317.6	4032.7	4186.2	4191.5	4126.5	4128.7	4109.1	4105.6
Ar		26134	26184.8	26130.3	26086.4	26144.3	26073.9	26057.4	26082.9
CO	132213.4	157368.9	161196.7	161094	160876.6	160840.8	160517.3	160499.8	160371.3
CH$_4$	74733.35	1361	1385.9	1338	1352.5	1360.6	1395.3	1400.6	1406.6
CO$_2$	564777.3	348.5	336.1	333.1	329.5	331.3	330.8	339.8	332.8

Min		15	30	45	60	75	90	105	120
	CO	0.0001460	0.0001496	0.0001495	0.0001493	0.0001493	0.0001490	0.0001890	0.0001880
Mole	CH$_4$	0.0000022	0.0000023	0.0000022	0.0000022	0.0000022	0.0000023	0.0000023	0.0000023
	CO$_2$	0.0000004	0.0000004	0.0000004	0.0000004	0.0000004	0.0000004	0.0000004	0.0000004
% CO conversion		14.33	12.42	12.29	12.26	12.47	12.41	12.37	12.52
% Selectivity	CH$_4$	85.51	86.17	85.86	86.12	86.13	86.44	86.17	86.46
	CO$_2$	14.49	13.83	14.14	13.88	13.87	13.56	13.83	13.54

Table B-4 Determination of CO conversion and gas product selectivity.

Data from the use of catalyst: 10wt% Co/ SiO$_2$ fiber catalyst

Temperature of reaction = 260°C

Feed flow rate 15 mL/min, Weight of catalyst = 0.2 g

Standard gas composition: 20wt% CO, 20wt% CH$_4$ 100wt% CO$_2$ balance in He

Area	std	15	30	45	60	75	90	105	120
H$_2$		4042.7	4007	3999.2	3882.2	3947.1	4029.1	4021.1	3975.7
Ar		27848.3	27643.8	27458.4	27282.2	27377.3	27364.6	27363	27282.2
CO	132730.1	160390.9	160468	159637.9	159812.7	159678.6	160511.1	160452.5	160319.7
CH$_4$	75120.65	765.5	843.6	873.2	947.2	995.1	1046.4	947.2	1012.2
CO$_2$	538540.2	288.1	269.3	237.9	187.3	251.3	209.6	197.1	199.6

Min		15	30	45	60	75	90	105	120
Mole	CO	0.0001482	0.0001485	0.0001476	0.0001475	0.0001473	0.0001483	0.0001486	0.0001483
	CH$_4$	0.0000013	0.0000014	0.0000014	0.0000015	0.0000016	0.0000017	0.0000015	0.0000017
	CO$_2$	0.0000003	0.0000003	0.0000003	0.0000002	0.0000003	0.0000002	0.0000002	0.0000002
% CO conversion		9.55	8.84	8.70	8.01	8.42	7.93	7.92	7.99
% Selectivity	CH$_4$	79.21	81.79	84.03	87.88	85.02	87.74	87.33	85.11
	CO$_2$	20.79	18.21	15.97	12.12	14.98	12.26	12.67	14.89

Table B-5 Determination of CO conversion and gas product selectivity.

Data from the use of catalyst: 10wt% Co/ SiO_2 fiber catalyst

Temperature of reaction = $280^{o}C$

Feed flow rate 15 mL/min, Weight of catalyst = 0.2 g

Standard gas composition: 20wt% CO, 20wt% CH_4 100wt% CO_2 balance in He

Area	std	15	30	45	60	75	90	105	120
H_2		3754.7	3773.9	3780.4	3767	3779.3	3710.6	3767.6	3746.7
Ar		27967.5	27779.5	27735.5	27692.3	27648.8	27578.1	27519.9	27509
CO	147422.9	159644.1	159486.3	160288.3	160035.6	160003.3	159307.7	159615.7	159254.5
CH_4	82670.8	1710.1	1817.7	1820.8	2059.7	2013.9	2068	2085.3	2146.9
CO_2	551982.35	310.8	378.5	394.4	371.3	321.2	315.8	304.4	391.9

Min		15	30	45	60	75	90	105	120
	CO	0.0001329	0.0001327	0.0001334	0.0001332	0.0001332	0.0001326	0.0001328	0.0001325
Mole	CH_4	0.0000025	0.0000027	0.0000027	0.0000031	0.000003	0.0000031	0.0000031	0.0000032
	CO_2	0.0000003	0.0000004	0.000004	0.0000004	0.0000004	0.0000004	0.0000003	0.0000004
% CO conversion		14.80	14.31	13.74	13.75	13.63	13.78	13.43	13.6
% Selectivity	CH_4	88.02	86.51	86.04	88.11	89.33	89.74	90.15	87.97
	CO_2	11.98	13.49	13.96	11.89	10.67	10.26	9.85	12.03

Table B-6 Determination of CO conversion and gas product selectivity.

Data from the use of catalyst: 10wt% Co/ SiO_2 fiber catalyst

Temperature of reaction = 300°C

Feed flow rate 15 mL/min, Weight of catalyst = 0.2 g

Standard gas composition: 20wt% CO, 20wt% CH_4 100wt% CO_2 balance in He

Area	std	15	30	45	60	75	90	105	120
H_2		3819.1	3838.8	3836.2	3832.9	3809.6	3823.5	3765.5	3804.4
Ar		27933.9	27930.1	27961.1	28662.6	28590.4	28532.7	27759.6	27729.3
CO	132213.4	157368.9	161196.7	161094	160876.6	160840.8	160517.3	160499.8	160371.3
CH_4	74733.35	2305.5	2547.1	2566.1	2586.5	2630.8	2657	2709.9	2566.1
CO_2	564777.3	480.4	505.3	496.1	534	539.5	515.5	542.4	487.9

Min		15	30	45	60	75	90	105	120
	CO	0.0001478	0.0001477	0.0001474	0.0001472	0.0001472	0.0001467	0.0001466	0.0001475
Mole	CH_4	0.0000038	0.0000042	0.0000042	0.0000042	0.000043	0.0000044	0.0000044	0.0000042
	CO_2	0.0000005	0.0000005	0.000005	0.0000006	0.0000006	0.0000006	0.0000006	0.0000005
% CO conversion		18.88	18.94	19.17	21.28	21.08	21.18	19.02	18.45
% Selectivity	CH4	87.88	88.40	88.66	87.98	88.05	88.62	88.31	88.83
	CO_2	12.12	11.60	11.34	12.02	11.95	11.38	11.69	11.17

Table B-7 Determination of CO conversion and gas product selectivity.

Data from the use of catalyst: 5wt% Co/ SiO_2 fiber catalyst

Temperature of reaction = 300^oC

Feed flow rate 15 mL/min, Weight of catalyst = 0.2 g

Standard gas composition: 20wt% CO, 20wt% CH_4 100wt% CO_2 balance in He

Area	std	15	30	45	60	75	90	105	120
H_2		3964.5	3930.8	3930.8	3945.8	3922.6	3911.4	3910.1	3926
Ar		26386.8	26378.1	26263.4	26203.7	26201.4	26159	26130.2	26139.3
CO	138828.35	158331.4	158230.8	158115.1	157845	157458.8	157134.3	157292.2	157406.9
CH_4	78990	1054.9	1219.1	1328	1352	1346.9	1369.7	1384.6	1389.3
CO_2	538540.2	328.2	345.3	347.3	373.1	370.5	354.2	333.9	363.6

Min		15	30	45	60	75	90	105	120
	CO	0.0001399	0.0001398	0.0001397	0.0001395	0.0001392	0.0001389	0.0001390	0.0001391
Mole	CH_4	0.0000016	0.0000019	0.0000021	0.0000021	0.0000021	0.0000021	0.0000022	0.0000022
	CO_2	0.0000004	0.0000004	0.0000004	0.0000004	0.0000004	0.0000004	0.0000004	0.0000004
% CO conversion		10.61	10.64	10.32	10.27	10.48	10.52	10.33	10.29
% Selectivity	CH_4	81.42	82.80	83.91	83.17	83.21	84.06	84.97	83.90
	CO_2	18.58	17.20	16.09	16.83	16.79	15.94	15.03	16.10

Table B-8 Determination of CO conversion and gas product selectivity.

Data from the use of catalyst: 15wt% Co/ SiO_2 fiber catalyst

Temperature of reaction = 300^oC

Feed flow rate 15 mL/min, Weight of catalyst = 0.2 g

Standard gas composition: 20wt% CO, 20wt% CH_4 100wt% CO_2 balance in He

Area	std	15	30	45	60	75	90	105	120
H_2		3738.8	3776.7	3703.8	3678.7	3771.2	3832.9	3820.9	3841.9
Ar		27265.1	26412.9	27384.5	28020.8	27897.3	27780.9	27759.6	27729.3
CO	131221.85	155160.4	155774.1	154814.5	154402.6	156139	157317	157026.4	157143.7
CH_4	74733.35	4081.1	3881.7	3861.8	3867.6	3694	3509.2	3403.1	3299.6
CO_2	563951.25	678.1	714.3	722.4	687.8	678.4	660	638.2	642.6

Min		15	30	45	60	75	90	105	120
	CO	0.0001451	0.0001456	0.0001448	0.0001444	0.0001460	0.0001471	0.0001468	0.0001469
Mole	CH_4	0.0000067	0.0000064	0.0000063	0.0000063	0.0000061	0.0000058	0.0000056	0.0000054
	CO_2	0.0000007	0.0000008	0.0000008	0.0000007	0.0000007	0.0000007	0.0000007	0.0000007
% CO conversion		10.82	7.58	11.41	13.65	12.29	11.26	11.36	11.19
% Selectivity	CH_4	90.08	89.13	88.97	89.46	89.15	88.92	88.95	88.57
	CO_2	9.92	10.87	11.03	10.54	10.85	11.08	11.05	11.43

Table B-9 Determination of CO conversion and gas product selectivity.

Data from the use of catalyst: 20wt% Co/ SiO$_2$ fiber catalyst

Temperature of reaction = 300°C

Feed flow rate 15 mL/min, Weight of catalyst = 0.2 g

Standard gas composition: 20wt% CO, 20wt% CH$_4$ 100wt% CO$_2$ balance in He

Area	std	15	30	45	60	75	90	105	120
H$_2$		3758.3	3735.2	3732.7	3728.6	3721.9	3704.9	3697.1	3683.6
Ar		27663.2	27744.1	27872.3	27988.7	28056.3	28019.7	27934.3	28029.8
CO	133243.8	157788	157668.2	157879.1	157858.2	157745.6	157531.6	157639.7	157501
CH$_4$	75849.45	5716.2	6016.2	6358.4	6541.8	6757.4	6918.6	7064	7110.5
CO$_2$	522486.2	943.8	984.9	1000.9	1033.1	1032.6	1005.5	1037.6	1027.8

Min		15	30	45	60	75	90	105	120
	CO	0.0001453	0.0001452	0.0001454	0.0001454	0.0001453	0.0001451	0.0001452	0.0001450
Mole	CH$_4$	0.0000092	0.0000097	0.0000103	0.0000106	0.0000109	0.0000112	0.0000114	0.0000115
	CO$_2$	0.0000011	0.0000012	0.0000012	0.0000012	0.0000012	0.0000012	0.0000012	0.0000012
% CO conversion		8.70	9.03	9.33	9.72	10.00	10.01	9.67	10.06
% Selectivity	CH$_4$	89.30	89.38	89.75	89.72	90.02	90.46	90.37	90.50
	CO$_2$	10.70	10.62	10.25	10.28	9.98	9.54	9.63	9.50

VITA

Miss Suwadee promduang was born on July 1, 1983 in Bangkok, Thailand. She graduated with Bachelor's degree of science, majoring in Chemistry, Faculty of Science, Mahidol University in 2006. After that, she worked as assistant teacher at Faculty of Science, King Mongkut's University of Technology Thonburi, during 2006-2007.Presence, she has been a graduate student in program of Petrochemistry and Polymer Science, Faculty of Science, Chulalongkron University, Bangkok, Thailand since 2007 and finished her study in 2010.

Presentation Experience

Poster presentation from The Pure and Applied Chemistry International Conference 2010 (PACCON2010) organized by Ubonratchathani University Thailand, 21-23 January, 2010 in the topic of "Preparation of Co/SiO$_2$ fiber catalyst by electrospinning".